Departament de Teoria
del Senyal i Comunicacions
UNIVERSITAT POLITÈCNICA DE CATALUNYA

MULTIDIMENSIONAL SPECKLE NOISE, MODELLING AND FILTERING RELATED TO SAR DATA

by

Carlos López Martínez

Xavier Fàbregas Cànovas, Thesis Advisor

Ph.D. Dissertation

Thesis Committee: Antoni Broquetas i Ibars
Ignasi Corbella i Sanahuja
Jong-Sen Lee
Eric Pottier
Juan Manuel López Sánchez

Barcelona, June 2, 2003

Chapter 2

SAR Remote Sensing

2.1 Synthetic Aperture Radar

Synthetic Aperture Radar (SAR) is a coherent, microwave imaging technique for producing a high spatial resolution representation of the Earth's surface reflectivity. The previous sentence reveals the importance of SAR systems in Remote Sensing nowadays.

SAR technology has some special characteristics that differentiate it from other remote sensing techniques, for instance optical imaging or radiometry. First of all, a SAR system gathers Earth's surface information within the microwave region of the spectra, hence, it has the capability to retrieve information which only manifests in this spectral region. In addition, as these systems are active, i.e., they provide their own illumination source, they are independent of natural processes as the day/night cycle or weather effects. Nevertheless, despite this difference, SAR technology has to be understood as complementary to other remote sensing techniques.

A SAR system is able to retrieve scene's reflectivity information. Due to a special complex processing technique, this reflectivity information is characterized by a very high spatial resolution. Therefore, this advantage or feature has to be maintained independently of the processing applied to data, in order to offer it to potential final users. Despite the SAR processing is performed in the complex plane, information from the final SAR images can only be extracted from amplitude. As it will be shown, phase information will be very important for the case of multidimensional SAR systems. Indeed, phase will be a valuable observable in terms of information content.

2.1.1 Basic Concepts on SAR

In a simple radar system, a pulsed microwave transmitter generates a high power radar pulse which is directed to the antenna through a microwave circulator. The radar antenna directs the pulse to the object of interest, which scatters off part of the energy to the antenna. The received energy at the antenna is redirected to the radar's receiver through the circulator to be recorded or processed. Generally, the radar is mounted on a moving platform, normally a plane or a satellite. As the radar moves along its flight direction, referred as *azimuth* or *along-track* dimension, it images a swath along the ground. The antenna beam is normally pointed slant-wise towards the ground, perpendicularly to the flight direction, defined as *range* or *across-track* dimension.

The radar's range resolution is defined as the minimum range separation of two points that can be separated and distinguished by the radar in the range dimension. Therefore, the range resolution δ_r

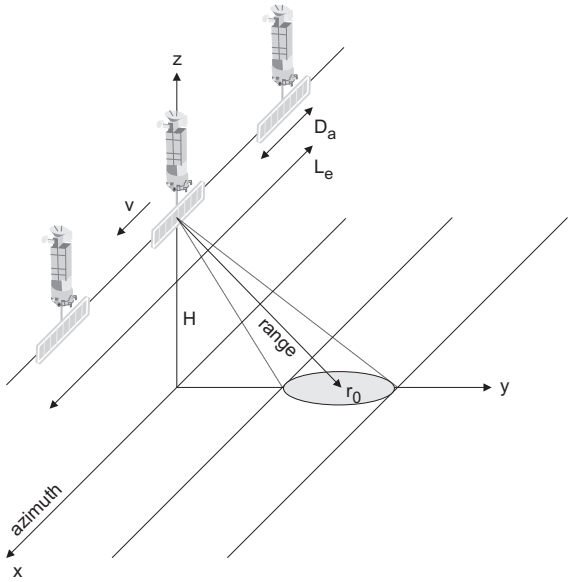

Figure 2.1: Synthetic Aperture Radar concept.

depends on the radar's pulse duration τ_p or inversely on the signal bandwidth B

$$\delta_r = \frac{c\tau_p}{2} = \frac{c}{2B} \tag{2.1}$$

where c denotes the propagation speed of Electromagnetic (EM) waves. In order to obtain a sufficient Signal to Noise Ratio (SNR) with short times τ_p, high energy pulses should be generated. As a big peak power cannot be achieved with practical transmitters, pulse compression techniques are employed [47]. These techniques are based on modulated long pulses to achieve large radiated energies, but simultaneously achieving the range resolution of short pulses. This is accomplished by means of frequency or phase modulation to widen the signal bandwidth B. The received pulse is processed in a matched filter [48, 49], compressing the long pulse to a duration $1/B$. All radar systems resolve targets in the range dimension in the same way. The way in which targets are resolved in the azimuth dimension makes the difference between SAR systems and other type of radars.

For a conventional radar, the antenna beam has an angular spread θ_a in the azimuth dimension proportional to

$$\theta_a \propto \frac{\lambda}{D_a} \tag{2.2}$$

where λ is the wavelength and D_a represents the antenna length in the azimuth dimension. Therefore, the resolution in the azimuth dimension δ_a becomes

$$\delta_a = r_0 \frac{\lambda}{D_a} \tag{2.3}$$

where r_0 represents the range distance between the antenna and the scatterer. For space applications, high spatial resolutions (i.e., tens of meters) can only be achieved using unpractical large antennas.

The azimuth resolution can be improved employing the synthetic aperture concept [50, 6, 51]. The SAR principle is based on using the platform's forward motion to construct a much longer effective antenna. This is done transporting the actual antenna to positions in which it can act as an individual element of a long linear array, giving finer resolutions in azimuth as shown by Fig. 2.1. Similarly, as for real aperture radar, the antenna beam spread θ_{sa}, corresponding to a synthetic antenna with a length L_e in the azimuth dimension, at a particular range r_0, is

$$\theta_{sa} = \frac{\lambda}{2L_e}. \tag{2.4}$$

The factor 2 accounts for the phase shift due to the two-way trip between the antenna and the scatterer. The azimuth resolution δ_a that can be achieved with the synthetic aperture is

$$\delta_a = r_0 \frac{\lambda}{2L_e}. \tag{2.5}$$

The maximum length of the synthetic aperture L_e, for a target at a range r_0, is limited by the amount of time the radar beam illuminates that target. This length corresponds to

$$L_e < \frac{\lambda R}{D_a}. \tag{2.6}$$

Consequently, the maximum achievable azimuth resolution δ_a with a synthetic aperture becomes

$$\delta_a > \frac{D_a}{2}. \tag{2.7}$$

It is worth to note, that for a SAR system, the azimuth resolution depends neither on the target's range position r_0 nor on the wavelength λ. It only depends on the azimuth antenna dimension D_a, in such a way that the smaller the antenna the better the resolution. The explanation for this rather surprising result lies in the fact that the length of the effective antenna is larger for farther scatterers than for closer ones.

2.1.2 SAR Impulse Response

The process to obtain a final SAR image is divided into two steps. The first step is the data acquisition process, in which EM pulses are transmitted by the system's antenna, scattered off by the imaged surface, received and finally recorded. The radar signal at this point is known as raw data. This signal, as it will be shown, does not have a direct relation with the surface's reflectivity. In order to obtain the reflectivity image it is necessary to focus the raw data signal through the so-called image formation process.

To understand completely the process to obtain a complex SAR image makes convenient to derive the SAR impulse response, that is, to obtain the response of a SAR system to a single or point scatterer, embracing, both, the acquisition, as well as the image formation processes. Finally, a complete image can be obtained as the superposition of the contributions of an arbitrary number of single scatterers. In this section, a strip map geometry for a SAR system, as presented by Fig. 2.2, will be considered. In

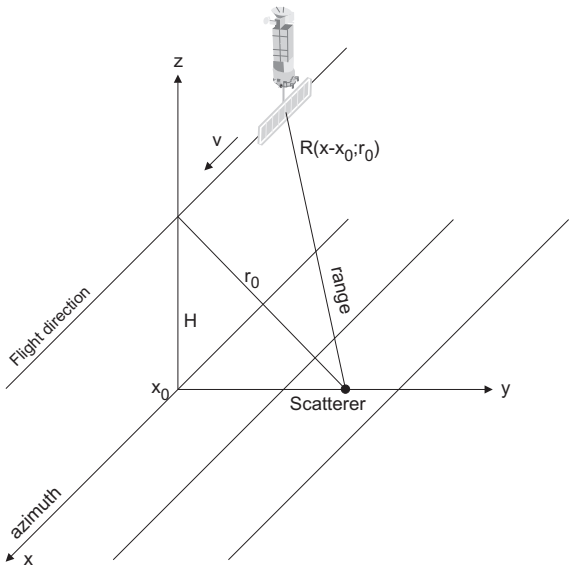

Figure 2.2: SAR stripmap geometry.

this configuration, the radar sensor moves at a constant velocity v along a straight trajectory, at a fixed attitude H (assuming no attitude errors), in the x dimension (azimuth or slow-time dimension). The radar will be assumed to point perpendicularly to one side of the flight line defining the second dimension r (range or fast-time dimension). Alternative SAR configurations for improved spatial resolution (spotlight SAR mode [52]) or for increased coverage (ScanSAR mode [53]) are also possible.

SAR data are defined in a two-dimensional space. There exist several ways to define its orthogonal dimensions. The first convention deals with time coordinates, defining the space as (t, τ), that is, slow-time and fast-time coordinates, respectively. The second convention takes into account spatial coordinates. In this case the signal space is defined as (x, r), azimuth and range respectively. In this text, the space convention will be employed as it allows to relate any expression with the position of a particular scatterer. Nevertheless, both conventions are related by

$$r = c\,2\tau \tag{2.8}$$
$$x = v\,t. \tag{2.9}$$

The time scales of these two dimensions differ from each other in several orders of magnitude allowing, on the one hand, to treat them as mutually independent and, on the other hand, to neglect the effect of the sensor's motion during the travelling time of a particular EM pulse. This assumption is often referred as *star-stop* approximation.

A point scatterer is defined in the two-dimensional space (x, r) as a Dirac's delta at the scatterer position (x_0, r_0)

$$\sigma_s(x_0, r_0) = \sqrt{\sigma} e^{j\theta} \delta(x - x_0, r - r_0) \tag{2.10}$$

where $\delta(x, r)$ is the two-dimensional Dirac's function. The function $\sigma_s(x_0, r_0)$ denotes the complex scattering amplitude, where σ is the complex radar cross section (RCS) [54, 47, 55] and θ is the scattering phase. The RCS is a measure of the strength of scattering from discrete reflecting objects, depending therefore, on its size, material, as well as on the imaging geometry, wavelength and polarization.

The SAR antenna transmits a series of EM pulses at a certain Pulse Repetition Frequency (PRF), modulated to a frequency carrier ω_o. In this text, only a singular pulse will be studied, as it is straightforward to obtain the response to a train of pulses. As it was pointed out within Section 2.1.1, phase coded EM pulses are employed to obtain high range resolution

$$s_t(t) = A(t) \exp(j(\omega_o t + \psi(t))) \tag{2.11}$$

where $A(t)$ represents the pulse amplitude and $\psi(t)$ is the pulse phase coding. $s_t(t)$ denotes the complex representation of the transmitted pulse. The pulse given by Eq. (2.11) interacts with a point scatterer, Eq. (2.10), located at (x_0, r_0). Assuming free-space propagation, the received echo can be written as

$$\begin{aligned} s_r(x, r; r_0) &= \sigma_s(x_0, r_0) w(x - x_0, r_0) A\left(\frac{2}{c}(r - R(x - x_0; r_0))\right) \\ &\cdot \exp\left(j\left(\omega_0\left(\frac{2}{c}(r - R(x - x_0; r_0)\right)\right) + j\psi\left(\frac{2}{c}(r - R(x - x_0; r_0))\right)\right) \end{aligned} \tag{2.12}$$

where $R(x - x_0; r_0)$ represents the sensor-to-scatterer distance (i.e., the range history), $w(x - x_0, r_0)$ denotes the illumination given by the antenna pattern (also including the range attenuation, system losses, system gain, etc...). After quadrature down-conversion [48], the carrier frequency ω_0 is removed and the received pulse, Eq. (2.12), becomes

$$\begin{aligned} s_r(x, r; r_0) &= \sigma_s(x_0, r_0) w(x - x_0, r_0) A\left(\frac{2}{c}(r - R(x - x_0; r_0))\right) \\ &\cdot \exp\left(j\psi\left(\frac{2}{c}(r - R(x - x_0; r_0))\right)\right) \exp\left(-j\frac{4\pi}{\lambda} R(x - x_0; r_0)\right). \end{aligned} \tag{2.13}$$

The expression given by Eq. (2.13) shows the way a SAR system encodes the signal returned by a point scatterer located at the position (x_0, r_0). Therefore, the point scatterer response of the SAR data acquisition system becomes

$$h_a(x, r; r_0) = w(x, r_0) A\left(\frac{2}{c}(r - R(x; r_0))\right) \exp\left(j\psi\left(\frac{2}{c}(r - R(x; r_0))\right)\right) \exp\left(-j\frac{4\pi}{\lambda} R(x; r_0)\right). \quad (2.14)$$

The previous expression can be divided into the convolution of two simpler transfer functions

$$\begin{aligned} h_a(x, r; r_0) &= h_{a1}(x, r; r_0) * h_{a2}(r) \\ h_{a1}(x, r; r_0) &= w(x, r_0) \exp\left(-j\frac{4\pi}{\lambda} R(x, r_0)\right) \delta(r - R(x, r_0)) \\ h_{a2}(r) &= A\left(\frac{2r}{c}\right) \exp\left(j\psi\left(\frac{2r}{c}\right)\right) \end{aligned} \quad (2.15)$$

where $*$ is the convolution operator. The transfer function $h_{a2}(r)$ depends only on the range dimension r. The range history $R(x; r_0)$ introduces a coupling between the range dimension r and the azimuth dimension x. The first effect of this double dependence is that the returned echo will not follow a straight line at the position r_0, but it will be placed within the hyperbolic curve defined by $R(x; r_0)$. This deviation from a straight line in the raw data is called Range Cell Migration (RCM). The range history $R(x; r_0)$ has a second noticeable effect on $h_{a1}(x, r; r_0)$ since it introduces an azimuth dependent phase history in a very sensitive way, called azimuth chirp. The SAR image formation process exploits this sensitive phase structure, performing a deconvolution in azimuth, to resolve different scatterers within the synthetic aperture. The existing coupling between range and azimuth makes SAR data processing a two-dimensional, non-separable problem.

The data acquisition point scatterer response of a SAR system, Eq. (2.14), spreads the complex reflectivity information about a single scatterer to an extensive region of the (x, r) plane. Hence, the raw data signal Eq. (2.13) has rather little relation with the scatterer reflectivity given by Eq. (2.10). To recover the point scatterer reflectivity, it is necessary to remove the effect of the acquisition process, Eq. (2.15), that is, to collect all the contributions of a particular scatterer and to focus them as good as possible.

The SAR data focusing process is most often divided into a range compression and an azimuth compression [6, 56]. Usually, matched filtering techniques [48, 49] are employed for this purpose, since it exist an exact knowledge about the transfer function to compensate, Eq. (2.14). Under the start-stop approximation, assuming no Doppler effects on individual pulses, the range compression can be simply performed, in a pulse by pulse basis, correlating the received pulse with the complex response $h_{a2}(r)$ located at the correct range position

$$A_c(t) = \int_{-\infty}^{\infty} h_{a2}(t - \tau) A(\tau) \exp\left(j\psi(\tau)\right) \mathrm{d}\tau. \quad (2.16)$$

Most often, linear chirp pulses are employed [47], in which the instantaneous frequency changes linearly with time

$$s_t(t) = \mathbf{1}_{[0,\tau]} \exp\left(j(\omega_o t + \alpha t^2/2)\right) \quad (2.17)$$

where $\mathbf{1}_{[0,\tau]}$ is a rectangular pulse of duration τ and α is the chirp rate related with the pulse bandwidth B by $\alpha\tau \simeq B$. In this case, the matched filter response is found to be

$$\begin{aligned} A_c(t) &= \frac{\sin(\pi\alpha t(\tau - |t|))}{\pi\alpha t}, |t| \leq \tau \\ &\simeq \tau \frac{\sin(\pi\alpha\tau\, t)}{\pi\alpha\tau\, t} = \tau \mathrm{sinc}(\pi\alpha\tau\, t). \end{aligned} \quad (2.18)$$

The expression $\sin(x)/x$ is the $\mathrm{sinc}(x)$ function, with a zero to zero width of $2/B$.

After applying the range compression process, Eq. (2.16), to the raw data signal, Eq. (2.13), the following signal is obtained

$$s_{rc}(x,r;r_0) = \sigma_s(x_0,r_0)w(x-x_0,r_0)A_c\left(\frac{2}{c}(r-R(x-x_0;r_0))\right)\exp\left(-j\frac{4\pi}{\lambda}R(x-x_0;r_0)\right). \tag{2.19}$$

The second step into the image formation process is the azimuth compression. This step has to compensate for the range-azimuth dependent phase history, Eq. (2.15). The reference signal is derived from the expression $h_{a1}(x,r;r_0)$ in Eq. (2.15). The range history $R(x,r_0)$, for a particular azimuth position, has the expression

$$R(x-x_0,r_0) = \sqrt{r_0^2+(x-x_0)^2} = \sqrt{r_0^2+v^2(t-t_0)^2} \tag{2.20}$$

where the azimuth dimension is expressed now in time coordinates t. This function expresses an hyperbolic curve in the plane (t,τ) with the apex at the position t_0. The hyperbolic expression can be simplified to a parabolic curve, determined by the Taylor expression expanded at the point (t_0,r_0), where the target is located at the center of the antenna beam

$$R(x-x_0,r_0) \simeq r_0 + \frac{v^2}{2r_0}(t-t_0)^2 \tag{2.21}$$

(t_0,r_0) are known as zero-Doppler coordinates.

The azimuth processing is performed correlating the received signal Eq. (2.19) with the expected signal for the point being processed. The reference signal $h_{a1}(x,r;r_0)$ for a particular point (x_1,r_1) was found in Eq. (2.15). If w_{ref} is defined as the reference azimuth weighting function, the complex output image $S(x_1,r_1)$ is found as

$$\begin{aligned} S(x_1,r_1) &= \int_{-\infty}^{\infty}\int_{-\infty}^{\infty} s_{rc}(x,r;r_0)h^*_{a1}(x-x_1,r;r1)\,\mathrm{d}x\,\mathrm{d}r \qquad (2.22)\\
&= \int_{-\infty}^{\infty}\int_{-\infty}^{\infty}\sigma_s(x_0,r_0)w(x-x_0,r_0)A_c\left(\frac{2}{c}(r-R(x-x_0;r_0))\right)\exp\left(-j\frac{4\pi}{\lambda}R(x-x_0;r_0)\right)\\
&\cdot\ w_{ref}(x-x_1;r_1)\delta\left(r-R(x-x_1;r_1)\right)\exp\left(j\frac{4\pi}{\lambda}R(x-x_1;r_1)\right)\mathrm{d}x\,\mathrm{d}r\\
&= \sigma_s(x_0,r_0)\int_{-\infty}^{\infty} w_{ref}(x-x_1;r_1)w(x-x_0,r_0)A_c\left(\frac{2}{c}\left(R(x-x_1;r_1)-R(x-x_0;r_0)\right)\right)\\
&\cdot\ \exp\left(j4\pi\frac{R(x-x_1;r_1)-R(x-x_0;r_0)}{\lambda}\right)\mathrm{d}x \end{aligned}$$

where $S(x,r)$ represents the final SAR image. Assuming that r_1 and r_0 are nearly equal, the range difference can be obtained, using Eq. (2.21), as

$$R(x-x_1;r_1)-R(x-x_0;r_0) \simeq \Delta r - \frac{x\,\Delta x}{r_0} + \frac{1}{2r_0}(x_1^2-x_0^2) \tag{2.23}$$

where $\Delta r = r_1 - r_0$ and $\Delta x = x_1 - x_0$. In order to derive the SAR impulse response, the following approximations will be assumed [57]:

· Since the antenna bandwidth is much wider than the impulse response

$$w(x-x_0,r_0)w_{ref}(x-x_1,r_1) \simeq w(x-x_0,r_0)w_{ref}(x-x_0,r_0) = w_{eff}(x-x_0,r_0). \tag{2.24}$$

· The series expansion of the range history Eq. (2.23) is valid to evaluate range-azimuth dependent phase history

$$\exp\left(j4\pi\frac{R(x-x_1;r_1)-R(x-x_0;r_0)}{\lambda}\right). \tag{2.25}$$

· The first term of the range history Eq. (2.23) is valid to describe the range difference when (x_0, x_0) and (x_1, x_1) are not much different

$$A_c\left(\frac{2}{c}\left(R(x-x_1,r_1)-R(x-x_0,r_0)\right)\right)=A_c\left(\frac{2}{c}\Delta r\right). \tag{2.26}$$

Taking Eq. (2.22), with the approximations given in Eqs. (2.24), (2.25) and (2.26), the complex output image $S(x_1, r_1)$ has the expression

$$S(x_1,r_1)=\sigma_s(x_0,r_0)A_c\left(\frac{2}{c}\Delta r\right)\exp\left(j\frac{4\pi}{\lambda}\Delta r\right)\int_{-\infty}^{\infty}w_{eff}(x-x_0,r_0)\exp(-j\,2\pi f x)\,\mathrm{d}x \tag{2.27}$$

where $f = 2\Delta x/\lambda r_0$ has been employed. As it can be deduced from Eq. (2.27), the response in azimuth depends on the Fourier transform of the product of the real and the processor antenna bandwidths. Thus, wide beams will give narrow responses. For the sake of simplicity, a square shaped antenna bandwidth will be assumed. For an antenna with an azimuth length D_a at the wavelength λ, the Fourier transform of the beam is

$$\int_{-\frac{\lambda r_0}{2D_a}}^{\frac{\lambda r_0}{2D_a}}w_{eff}(x-x_0,r_0)\exp(-j\,2\pi f x)\,\mathrm{d}x=\frac{\lambda r_0}{D_a}\frac{\sin(\pi f\frac{\lambda r_0}{D_a})}{\pi f\frac{\lambda r_0}{D_a}}w=\frac{\lambda r_0}{D_a}\,\mathrm{sinc}\left(2\pi\frac{\Delta_x}{D_a}\right). \tag{2.28}$$

Using Eqs. (2.18), (2.27) and (2.28), taking into account the resolution definitions in range, Eq. (2.1), and azimuth Eq. (2.7), the output SAR complex image, for a point scatterer located at the coordinates (x_0, r_0), has the expression

$$S(x,r)=\sigma_s(x_0,r_0)\exp\left(j\frac{4\pi}{\lambda}(r-r_0)\right)\mathrm{sinc}\left(\frac{\pi(r-r_0)}{\delta_r}\right)\mathrm{sinc}\left(\frac{\pi(x-x_0)}{\delta_a}\right). \tag{2.29}$$

Therefore, the impulse response of the SAR chain, embracing the data acquisition, as well as the image formation processes, is proportional to the expression

$$h(x,r)\propto\exp\left(j\frac{4\pi}{\lambda}r\right)\mathrm{sinc}\left(\frac{\pi r}{\delta_r}\right)\mathrm{sinc}\left(\frac{\pi x}{\delta_a}\right). \tag{2.30}$$

The SAR system response, embracing the acquisition and the focussing processes, can be therefore assumed as a rectangular filter with a range bandwidth equal to $2B/c$ and an azimuth bandwidth equal to $2/D_a$ [6, 56, 58]. In the process of deriving the Eq. (2.30), the constant phase term from range delay, $\exp(j\,4\pi r/\lambda)$, has been assigned to the SAR system. This phase term can also be assigned to the scene, introduced as $\exp(-j\,4\pi r/\lambda)$. Thus, the SAR impulse response is simply proportional to

$$h(x,r)\propto\mathrm{sinc}\left(\frac{\pi r}{\delta_r}\right)\mathrm{sinc}\left(\frac{\pi x}{\delta_a}\right). \tag{2.31}$$

Fig. 2.3 shows which is the aspect of the SAR impulse response at different points of the processing chain.

2.1.3 SAR Imaging System Model

As shown in the previous section, the SAR impulse response effect is to convolve the scene's reflectivity with a low-pass filter. Since the spatial dimensions of this filter are not equal to zero, the concept of resolution cell can be defined as the area given by the SAR impulse response, i.e., the area $\delta_a \times \delta_r$. For a real situation, the received echo is not due to a single scatterer, but to the combination of the echoes of an arbitrary number of point scatterers inside this resolution cell [59, 55]. All these small scatterers are located at random positions inside the resolution cell, radiating perhaps random complex echoes.

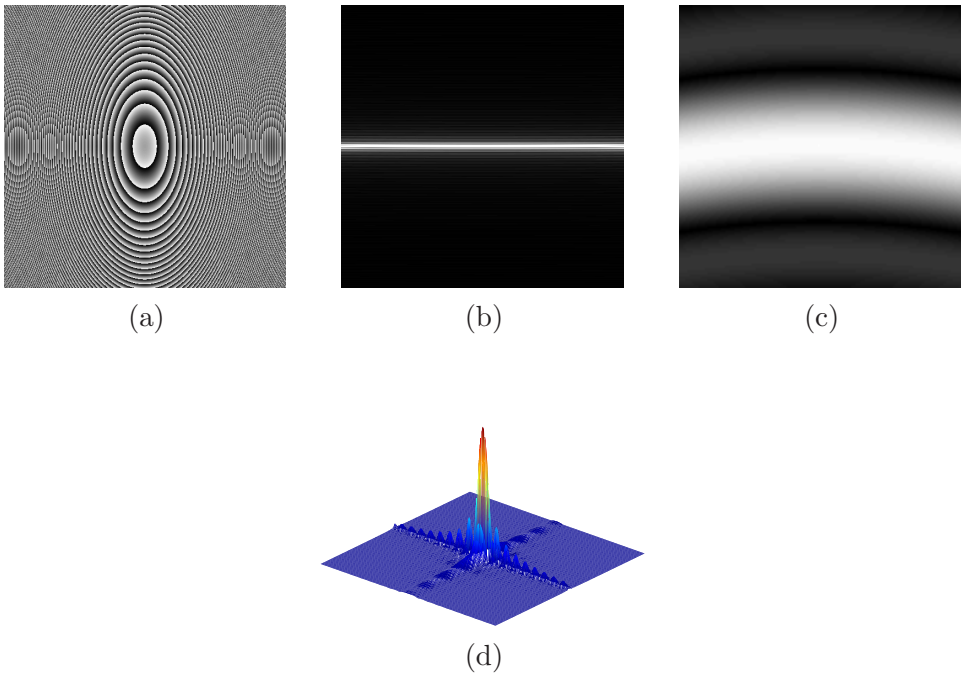

(a) (b) (c)

(d)

Figure 2.3: SAR raw data focusing steps for a point scatterer. (a) Raw data (phase). (b) Data after range compression. (c) Range cell migration detail. (d) Data after azimuth compression (SAR two-dimensional impulse response).

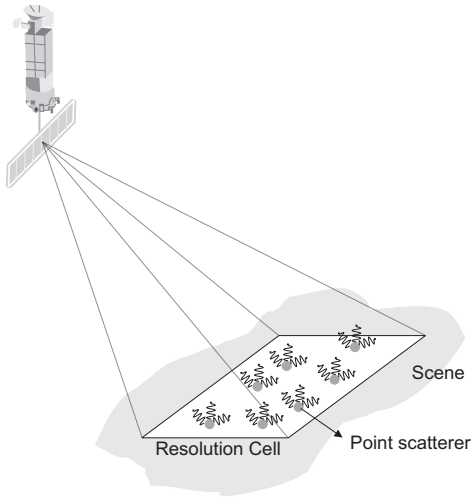

Figure 2.4: Distributed scatterer scheme.

The randomness involved within the scattering process makes evident that it can be only characterized statistically [57, 55, 60]. These scatterers, as shown by Fig. 2.4, characterized by having a random behavior, are called distributed or partial scatterers, as opposed to point scatterers Eq. (2.10), in which the scattering behavior is completely deterministic.

The set of point scatterers defining a distributed scatterer can be described, in a three-dimensional space, by means of the complex reflectivity function $\widetilde{u}(x, y, z)$ [57, 61, 62]. As mentioned in the previous paragraph, this reflectivity function has a random nature. The development of the SAR system model only needs $\widetilde{u}(x, y, z)$ as a function describing the reflectivity of each point scatterer. The statistical properties of $\widetilde{u}(x, y, z)$ will be studied in the following.

In order to arrive to a simple model characterizing the SAR system, it is necessary to assume linearity in the scattered field. There exist several approximations in the classical scattering theory allowing to know the scattered field by a complex scatterer. Within the Kirchhoff approximation, for instance,

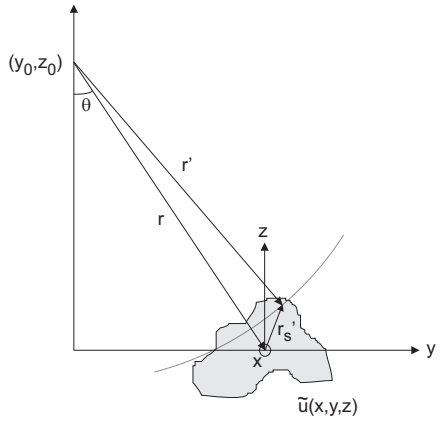

Figure 2.5: Distributed scatterer imaging geometry.

the scattered field is replaced by its geometrical optics approximation [63]. The development of the SAR system model will be based, on the other hand, on the Born approximation, or single scattering approximation [64, 63]. In this case, the total scattered field will be assumed to be the superposition of the scattered field by each simple scatterer, neglecting thus, high order interactions, as for instance double reflections.

A SAR system, as seen in Section 2.1.2, gathers reflectivity data in the range-azimuth space. The first step a SAR system performs is to transform the three dimensional reflectivity function $\widetilde{u}(x, y, z)$ into the two-dimensional SAR system space (x, r), as presented by Fig. 2.5. This step can be seen as a projection function

$$\widetilde{u}(x, r) = \int \widetilde{u}(x, y_0 + r \sin\theta, z_0 - r\cos\theta) r \, \mathrm{d}\theta \tag{2.32}$$

where θ denotes the angle between the sensor-to-scatterer line and the z-axis. Under the Born scattered field approximation, the linear operation characterizing the SAR imaging process is a geometric projection of the reflectivity function $\widetilde{u}(x, y, z)$ given by Eq. (2.32) followed by a convolution with the SAR point response Eq. (2.31)

$$S(x, r) = \left(\int_{-\infty}^{\infty} \widetilde{u}(x, y_0 + r \sin\theta, z_0 - r\cos\theta) r \, \mathrm{d}\theta \right) * * h(x, r). \tag{2.33}$$

The projection process Eq. (2.33) does not affect the azimuth dimension x. On the contrary, it introduces several distortions in the range dimension r. The SAR systems gathers information along the r dimension, also known as *slant range* and not in the y dimension over the Earth's surface, known as *ground range*. Therefore, the integration over the angle θ, for a particular range coordinate, provokes all the scatterers located at this particular range to be integrated together and mapped within the same SAR image position. For terrain slopes tilted towards the SAR system, the projection makes them to appear contracted (foreshortening) in the image, while terrain slopes tilted away from the SAR get stretched. Once the terrain slope is equal or even exceeds the look angle θ, the projection becomes ambiguous, for instance, a mountain peak may be mapped onto the same pixel as some point in a valley. This effect is known as layover. For terrain slope angles minor than $\theta - \pi/2$, radar shadow is observed.

The complex SAR image, under the Born approximation, can be written as

$$S(x, r) = \int_{-\infty}^{\infty} \int_{-\infty}^{\infty} \widetilde{u}(x', r') \exp(-j2kr') h(x - x', r - r') \, \mathrm{d}x' \, \mathrm{d}r'. \tag{2.34}$$

In this equation, the variables (x, r) refer to the image dimensions, whereas the prime co-ordinates (x', r') indicate the position of a particular scatterer within the resolution cell, as shown by Fig. 2.5. At the same time, Eq. (2.34) can be rewritten as a volume integral

$$S(x, r) = \int_{V'} \widetilde{u}(x', y', z') \exp(-j2kr'(y', z')) h(x - x', r - r'(y', z')) \, \mathrm{d}V'. \tag{2.35}$$

In order to obtain a simple expression for Eq. (2.35), having an easy interpretation about the effect of the SAR impulse response, it is helpful to develop a planar wave approximation for the reflected waves [63,65]. The cylindrical wave expressed by the phase term $\exp(-j2kr')$ in Eq. (2.35) can be approximated by a planar wave considering only a sufficiently small neighborhood about an expansion point. The range r', which refers to any scatterer within the resolution cell, can be approximated as

$$r' \simeq r + \overrightarrow{k} \cdot \overrightarrow{r}'_s \tag{2.36}$$

where r represents the center of the resolution cell, $\overrightarrow{k} = k[0, \sin(\theta), -\cos(\theta)]^T$ and $\overrightarrow{r}'_s$ is the position vector of a particular scatterer respect to the resolution cell center. The variable k is the wavenumber equal to $2\pi/\lambda$ and ^{T} denotes transpose. Finally, substituting the cylindrical wave by its planar approximation, the complex SAR image becomes

$$\begin{aligned} S(x,r) &= \exp(-j2kr) \int_{V'} \widetilde{u}(x',y',z') \exp(-j2\overrightarrow{k} \cdot \overrightarrow{r}'_s) h(x-x', r-r'(y',z'))\, \mathrm{d}V' \\ &= \left\{ \exp(-j2kr) \int \widetilde{u}(x, y_0 + r\sin(\theta), z_0 - r\cos(\theta)) r\, \mathrm{d}\theta \right\} * * h(x,r). \end{aligned} \tag{2.37}$$

2.1.4 SAR Image Statistics

Most of natural targets have a very complex structure. Consequently, the knowledge of the scattered field would only be possible if a complete description of the scene was available, which is impossible in practice. Thus, this type of scatterers can only be described statistically. There exist two main types of wave scattering processes for distributed or partial scatterers: surface and volume scattering [66]. The former is produced when an EM wave reaches the boundary surface between two media and the scattering takes only place at the surface's boundary. In this case, the surface is described by the surface height standard deviation and the surface correlation length. On the contrary, volume scattering occurs when the EM wave penetrates into the lower medium. The scattering within a volume is mainly caused by randomly located dielectric discontinuities in the volume. This type of scatterers is described by statistical parameters as the average dielectric constant or the scatterer density. Apart from the mentioned factors, the scattering process depends also on other scatterer parameters as the composition, material, water content, etc...

SAR systems are mainly employed for natural scenes observation. Owing to the complexity of such a targets, the scattered EM wave has also a complex behavior [59, 67, 60]. Hence, the scattering process is also analyzed statistically. Most of the techniques focused on finding the scattered wave problem try to find the average scattered field as a function of the incident wave and the statistical properties of the scatterer.

The resolution cell dimensions are very large compared with the wavelength of the illuminating EM wave. Hence, as described in Section 2.1.3, the scattered field for a particular image pixel can be seen as being originated by the contribution of many elementary scattered waves. The monochromatic coherent nature of SAR systems makes all these elementary waves to interfere between them constructively as well as destructively, causing the SAR image to look noisy and grainy. Such a phenomenon is defined as *speckle* [6,8,7,68]. Despite being an electromagnetic measurement, speckle can be treated as a noise-like process as is will be shown in the following. The speckle is a common effect appearing in all those science disciplines based on imaging systems with a coherent illumination as laser optics [5, 3, 4], ultrasound imaging [69] or X-ray imaging.

Summarizing, due to the lack of knowledge about the detailed structure of the scatterer being imaged by the SAR system, it is necessary to discuss the properties of the scattered field statistically. The statistics of concern are defined over an ensemble of objects, all with the same *macroscopic* properties, but differing in the internal structure. For a given SAR system imaging a particular scatterer, for

instance a rough surface, the exact value of each pixel can not be predicted, but only the parameters of the distribution describing the pixel values. Therefore, for a SAR image, the actual information per pixel is very low as individual pixels are simply random samples from distributions characterized by a set of parameters.

In Section 2.1.2, it has been established that the SAR imaging process can be modelled as a two-dimensional low-pass filter applied to the scene's reflectivity, Eq. (2.37). The complex SAR image $S(x, r)$ can be modelled as

$$S(x,r) = \int_{-\infty}^{\infty}\int_{-\infty}^{\infty} \sigma_s(x', r')h(x - x', r - r')\,\mathrm{d}x'\,\mathrm{d}r' \tag{2.38}$$

where $h(x, r)$ denotes the coherent SAR impulse response and $\sigma_s(x', r')$ describes each one of the point scatterers inside the resolution cell. This model might be reasonable for those cases in which this point scatterer description is valid, as for instance, the scattering from raindrops or vegetation-covered surfaces having leaves small compared with the wavelength. On the contrary, this model is not valid for continuous targets. In these cases, it is helpful to apply the concept of *effective scattering center* [55], in which the continuous target is analyzed in a discrete way, e.g: the facet-model for surface scattering [59, 55]. Assuming the scattering from any complex target to be originated by a set of discrete sources, Eq. (2.38) can be written as

$$S(x,r) = \sum_{k=1}^{N} \sigma_s(x_k, r_k)h(x - x_k, r - r_k) \tag{2.39}$$

where the SAR impulse response h is supposed to be finite, embracing N point scatterers. Eq. (2.39) can be rewritten by using

$$\sigma_s(x_k, r_k) = \sqrt{\sigma_k}\exp(j\,\theta'_{s_k}) \tag{2.40}$$

$$h(x - x_k, r - r_k) = h_k \exp(j\,\varphi_k) \tag{2.41}$$

$$\theta_{s_k} = \theta'_{s_k} + \varphi_k \tag{2.42}$$

and the complex description, where r denotes amplitude and θ is the phase

$$S(r,\theta) = \Re\{S\} + j\,\Im\{S\} = r\exp(j\,\theta) \tag{2.43}$$

as

$$r\exp(j\,\theta) = \sum_{k=1}^{N} h_k\sqrt{\sigma_k}\exp(j\,\theta_{s_k}) \tag{2.44}$$

$$\Re\{S\} = \sum_{k=1}^{N} h_k\sqrt{\sigma_k}\cos(\theta_{s_k}) \tag{2.45}$$

$$\Im\{S\} = \sum_{k=1}^{N} h_k\sqrt{\sigma_k}\sin(\theta_{s_k}). \tag{2.46}$$

In [57], it was proved that the effect of the SAR system, through the amplitude h_k, is just to change the distribution of the amplitudes of the individual contributors to the complex sum Eq. (2.44). Therefore, this complex sum can be analyzed as

$$r\exp(j\,\theta) = \sum_{k=1}^{N} A_k\exp(j\,\theta_{s_k}) \tag{2.47}$$

$$\Re\{S\} = \sum_{k=1}^{N} A_k\cos(\theta_{s_k}) \tag{2.48}$$

$$\Im\{S\} = \sum_{k=1}^{N} A_k\sin(\theta_{s_k}) \tag{2.49}$$

where $A_k = h_k\sqrt{\sigma_k}$. The complex sum given by Eq. (2.47), also known as two-dimensional *random walk* [70, 71] can be seen graphically in Fig. 2.6.

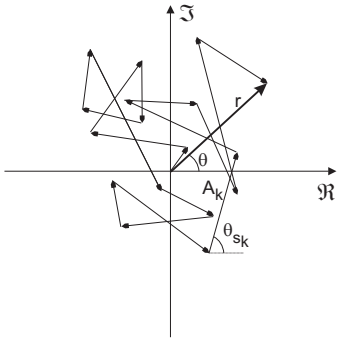

Figure 2.6: Two-dimensional random walk modelling the returned echo from a distributed scatterer.

To obtain the statistics of the complex SAR image $S(x, r)$ is based on certain assumptions concerning the behavior of the elementary complex scattered waves $A_k \exp(j\,\theta_{s_k})$. These assumptions are crucial, as all the statistics concerning SAR images are based on them [59, 4]:

- The amplitude A_k and the phase θ_{s_k} of the kth elementary phasor (i.e., elementary scattered wave) are statistically independent of each other and from the amplitudes and phases of all other elementary phasors. This fact states that the elementary scattering centers are uncorrelated and that the strength of a given scattered component bears no relation to its phase.
- The phases of the elementary contributions are equally likely to lie anywhere in the primary interval, $[-\pi, \pi)$.

These two assumptions are justified in the case of a SAR image provided the resolution cell dimensions to be larger than the EM wave wavelength. The first assumption is accomplished as the propagation phase delay is independent from the scattered wave strength. The second point is reasonable since the resolution cell dimensions are larger than the wavelength, introducing a very large range of total phase shift for point scatterers, leading to the phase to be uniformly distributed when folded in the interval $[-\pi, \pi)$. From the second assumption, it can be established that the phase due to the deterministic SAR impulse response φ_k does not have effect over the final phase distribution as it is randomized by the uniform phase distribution of the point scatterers θ'_{s_k}.

When the number of scatterers inside the resolution cell N is large, provided that $A_k \cos(\theta_{s_k})$ and $A_k \sin(\theta_{s_k})$ satisfy the Central Limit Theorem [72], the quantities $\Re\{S\}$ and $\Im\{S\}$ are normally distributed [59, 3, 4, 72], that is, they follow a zero-mean, Gaussian probability density function (pdf). The Gaussian pdf parameters can be obtained on the basis of the individual scatterers model. The mean values of $\Re\{S\}$ and $\Im\{S\}$ are obtained as

$$E\left\{\Re\left\{S\right\}\right\} = \sum_{k=1}^{N} E\left\{A_k \cos(\theta_{s_k})\right\} = \sum_{k=1}^{N} E\left\{A_k\right\}\, E\left\{\cos(\theta_{s_k})\right\} = 0 \tag{2.50}$$

$$E\left\{\Im\left\{S\right\}\right\} = \sum_{k=1}^{N} E\left\{A_k \sin(\theta_{s_k})\right\} = \sum_{k=1}^{N} E\left\{A_k\right\}\, E\left\{\sin(\theta_{s_k})\right\} = 0 \tag{2.51}$$

where $E\{\cdot\}$ expresses the ensemble average. Using the same arguments, the variance values are obtained as

$$E\left\{\Re^2\left\{S\right\}\right\} = \sum_{k=1}^{N} E\left\{A_k^2\right\}\, E\left\{\cos^2(\theta_{s_k})\right\} = \frac{N}{2} E\left\{A_k^2\right\} \tag{2.52}$$

$$E\left\{\Im^2\left\{S\right\}\right\} = \sum_{k=1}^{N} E\left\{A_k^2\right\}\, E\left\{\sin^2(\theta_{s_k})\right\} = \frac{N}{2} E\left\{A_k^2\right\}. \tag{2.53}$$

Besides, the correlation between $\Re\{S\}$ and $\Im\{S\}$ is

$$E\left\{\Re\left\{S\right\}\Im\left\{S\right\}\right\} = \sum_{k=1}^{N}\sum_{l=1}^{N} E\left\{A_k\, A_l\right\} E\left\{\cos(\theta_{s_k})\sin(\theta_{s_l})\right\} = 0. \tag{2.54}$$

This result follows from the symmetry of the phase pdf of the elementary scatterers [59]. If $\Re\{S\}$ is renamed as x and $\Im\{S\}$ is renamed as y, their pdfs are respectively

$$p_x(x) = \frac{1}{\sqrt{\pi\sigma^2}}\exp\left(-\left(\frac{x}{\sigma}\right)^2\right) \qquad x \in (-\infty, \infty) \tag{2.55}$$

$$p_y(y) = \frac{1}{\sqrt{\pi\sigma^2}}\exp\left(-\left(\frac{y}{\sigma}\right)^2\right) \qquad y \in (-\infty, \infty) \tag{2.56}$$

where $\sigma^2/2 = (N/2)\,E\left\{A_k^2\right\}$, as it was shown by Eqs. (2.52) and (2.53). The pdfs $p_x(x)$ and $p_y(y)$ correspond to zero-mean Gaussian distributions, denoted by $\mathcal{N}(0, \sigma^2/2)$. Consequently, a SAR image $S = x + jy$ is described by a zero-mean, complex, Gaussian pdf with the properties given from Eq. (2.50) to Eq. (2.54) and denoted in the following as $\mathcal{N}_c(0, \sigma^2/2)$. From Eqs. (2.55) and (2.56), it is straightforward to derive the amplitude pdf $p_r(r)$, where $r = \sqrt{x^2 + y^2}$, and the phase pdf $p_\theta(\theta)$, where $\theta = \arctan(y/x)$

$$p_{r,\theta}(r, \theta) = \frac{2r}{2\pi\sigma^2}\exp\left(-\frac{r^2}{\sigma^2}\right) \tag{2.57}$$

$$p_r(r) = \frac{2r}{\sigma^2}\exp\left(-\frac{r^2}{\sigma^2}\right) \qquad r \in [0, \infty) \tag{2.58}$$

$$p_\theta(\theta) = \frac{1}{2\pi} \qquad \theta \in [-\pi, \pi). \tag{2.59}$$

As it can be seen, the amplitude and phase distributions are separable. $p_r(r)$ is known as a Rayleigh distribution, whereas the phase is uniformly distributed. This fact is very important as it indicates that the SAR image phase is scatterer independent, that is, it has no information about the scatterer. The mean value of a Rayleigh distribution equals $E\{r\} = \sqrt{\pi\sigma^2}/2$, and a variance $\sigma_r^2 = (1 - (\pi/4))\sigma^2$. Another commonly used statistic is the Coefficient of Variation (CV), defined as the standard deviation divided by the mean [7]. Hence, for the amplitude r, the CV has a value equal to $\sqrt{(4/\pi) - 1}$. Normally, interest is focused on the intensity, i.e., $I = r^2$. Introducing this change of variable into Eq. (2.57), the intensity distribution becomes

$$p_I(I) = \frac{1}{\sigma^2}\exp\left(-\frac{I}{\sigma^2}\right) \qquad I \in [0, \infty) \tag{2.60}$$

which is an exponential distribution. Its mean value equals $E\{I\} = \sigma^2$, and the standard deviation is $\sigma_I^2 = \sigma^2$. Therefore, the intensity has a CV equal to 1. Fig. 2.7 gives some examples of the distributions of the amplitude r, intensity I and phase θ for complex SAR images for several values of σ.

The validity of the statistical distribution for the SAR images, is subjected to the assumptions taken to arrive to the zero-mean, Gaussian model for the SAR image real and imaginary parts, Eqs. (2.55) and (2.56), which will be referred as Gaussian scattering assumption in the following [59, 55]. It is important to note here, that concerning the process to arrive to this model, any assumption was taken with respect to the pdfs of the quantities A_k and θ_{s_k}. The crucial point for the development of the Gaussian Scattering Model was to assume the number of scatterers N large enough to fulfill the Central Limit Theorem.

When the number of scatterers N is large enough, as it has been shown in the previous paragraphs, the amplitude is described by a Rayleigh pdf and the phase is uniformly distributed. This situation is referred as fully developed speckle [13, 55]. In this case, the speckle noise is understood as the random variation with a Rayleigh distribution around the mean value $E\{r\} = \sqrt{\pi\sigma^2}/2$. To determine the value

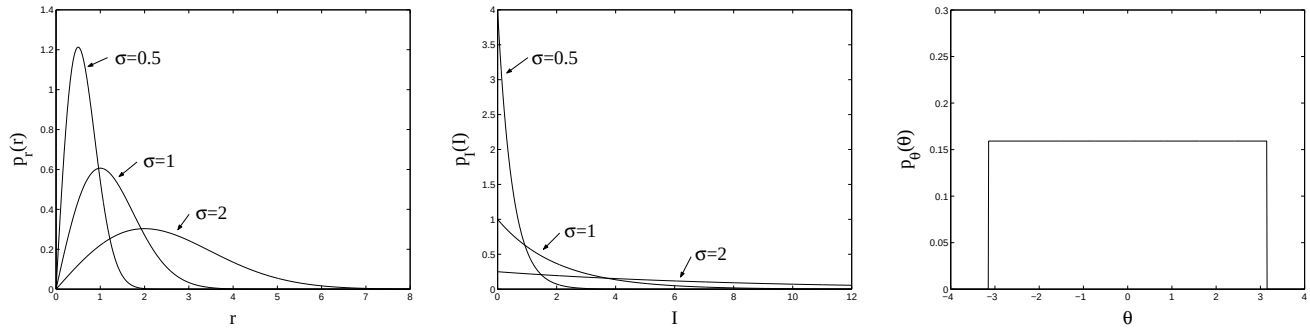

(a) (b) (c)

Figure 2.7: Complex SAR image distributions for several values of σ. (a) Amplitude. (b) Intensity. (c) Phase.

of N that makes the Central Limit Theorem to be fulfilled is impossible as no information about the distributions of A_k and θ_{s_k} is available. Besides, the value of N is not constant. For a general value of N, the square of the intensity CV has the value

$$\frac{\sigma_I^2}{E\{I\}^2} = 1 + \frac{2\text{var}\{N\}}{E\{N\}^2} + \frac{1}{E\{N\}}\left(\frac{\text{var}\{A_i^2\}}{E\{A_i^2\}^2} - 1\right). \tag{2.61}$$

If the individual scatterers are Rayleigh distributed or if $E\{N\}$ is large, Eq. (2.61) becomes

$$\frac{\sigma_I^2}{E\{I\}^2} = 1 + \frac{2\text{var}\{N\}}{E\{N\}^2}. \tag{2.62}$$

In many occasions, the value of N is assumed to follow a Poison distribution [7]. In this case, the Eq. (2.61) becomes

$$\frac{\sigma_I^2}{E\{I\}^2} = 1 + \frac{2}{E\{N\}}. \tag{2.63}$$

Thus, provided that $E\{N\} \to \infty$, the SAR image can be modelled by $\mathcal{N}_c(0, \sigma^2/2)$. In all these cases, any variation from 1 will mean that the Gaussian Scattering Model will not be valid.

For high spatial resolution SAR images, the Gaussian Scattering Model is not fulfilled when a few strong scatters are present within the resolution cell (e.g., urban areas). This case is referred, therefore, as partially developed speckle [13]. In the extreme case of an isolated point target, the value of this pixel is dominated by the deterministic impulse response of the SAR system, as shown in Eq. (2.29).

The validity of the Gaussian Scattering Model for SAR imagery has been largely demonstrated. Many studies in the literature support the Gaussian distribution for experimental SAR data [9, 57, 73].

2.1.5 Speckle Second Order Statistics

In the previous section, the reflectivity scene has been modelled as a large number of point scatterers, which are independent and randomly located in space. Hence, a complex backscattering coefficient per area, $\widetilde{u}(x, y)$, can be modelled by

$$\widetilde{u}(x, r) = \sum_{k=1}^{N} \sqrt{\sigma_k}\exp(j\theta_{s_k})\delta(x - x_k, r - r_k) \tag{2.64}$$

where $\delta(x, r)$ is the two-dimensional Dirac delta function, and N represents the number of scatterers in a particular scene area.

As mentioned, due to the complexity involved in the scattering process, it is impossible to predict the scattered field exact value. Only the average scattered power can be predicted. In order to describe it, the differential scattering coefficient or average scattering coefficient per unit area is defined as [55]

$$\sigma^0 = E\left\{\frac{\sigma}{\Delta A}\right\} \tag{2.65}$$

where ΔA denotes an spatial area. Here the expectation $E\{\cdot\}$ is assumed to be calculated in the spatial domain. The concept of average scattering coefficient is defined for surface scattering. When the dominant scattering mechanism is a volume scattering, a similar coefficient to σ^0, called volume scattering coefficient, and denoted by $\sigma_v(x,r)$, has been also defined [74].

To arrive to the reflectivity scene model given by Eq. (2.64) it has been assumed: a large number of scatterers per area and that these scatterers are independent with uniformly distributed phase. With these assumptions, the process $\widetilde{u}(x,r)$ can be described by a zero-mean, complex, Gaussian pdf. The process $\widetilde{u}(x,r)$ can not be observed itself, but it has been established that this process observed through a SAR system, which has a linear impulse response, can be modelled as a zero-mean, complex, Gaussian process. Therefore, it can be considered that $\widetilde{u}(x,r)$ is also a zero-mean, complex, Gaussian process [57]. The process $\widetilde{u}(x,r)$ is described by the autocorrelation function

$$E\left\{\widetilde{u}(x_1,r_1)\widetilde{u}^*(x_2,r_2)\right\} = R_{\widetilde{u}}(x_1,r_1,x_2,r_2) = \sigma^0(x_2,r_2)\delta\left(x_1-x_2,r_1-r_2\right). \tag{2.66}$$

For an homogeneous scene, the autocorrelation becomes

$$R_{\widetilde{u}}(x_1,r_1,x_2,r_2) = \sigma^0\delta\left(x_1-x_2,r_1-r_2\right) \tag{2.67}$$

with the corresponding spectral density function

$$G_{\widetilde{u}}(f_x,f_r) = \int_{-\infty}^{\infty} R_{\widetilde{u}}(x,r)\exp(-j\pi(xf_x+rf_r))\,\mathrm{d}x\,\mathrm{d}r = \sigma^0. \tag{2.68}$$

The autocorrelation and spectral density functions given by Eqs. (2.67) and (2.68) respectively, close the model for the reflectivity scene. As it has been highlighted, the reflectivity scene can be modelled as a collection of uncorrelated point scatterers, randomly located and described by a zero-mean, complex, Gaussian pdf and in the autocorrelation function given by Eq. (2.67).

The effect of the SAR system has been already seen in the previous sections. The main effect is to convolve the scene reflectivity with a two-dimensional low-pass filter. Now, the reflectivity scene model shown before, will be employed to characterize the complex SAR image autocorrelation function. The previous section showed that the SAR system impulse response has no effect on the first-order statistics of the SAR image, which can be modelled by $\mathcal{N}_c(0,\sigma^2/2)$. On the contrary, the second order statistics of the SAR image are completely determined by the SAR system impulse response. From signal processing, the autocorrelation and spectral density functions of the output signal $S(x,r)$ of a linear system characterized by the impulse response $h(x,r)$, excited by the signal $\widetilde{u}(x,r)$ are respectively [72]

$$R_S(x,r) = \int_{-\infty}^{\infty}\int_{-\infty}^{\infty} R_{\widetilde{u}}(x-x',r-r')h(x',r')\,\mathrm{d}x'\,\mathrm{d}r' \tag{2.69}$$

$$G_S(f_x,f_r) = G_{\widetilde{u}}(f_x,f_r)\left|H(f_x,f_r)\right|^2 \tag{2.70}$$

where $H(f_x,f_r)$ denotes the Fourier transform of the impulse response $h(x,r)$. Using the autocorrelation function given by Eq. (2.66), the autocorrelation and the spectral density functions of the SAR image $S(x,r)$ are

$$R_S(x,r) = \sigma^0 R_h(x,r) \tag{2.71}$$

$$G_S(f_x,f_r) = \sigma^0\left|H(f_x,f_r)\right|^2. \tag{2.72}$$

where

$$R_h(x,r) = \int_{-\infty}^{\infty}\int_{-\infty}^{\infty} h(s,t)h^*(s-x,t-r)\,\mathrm{d}s\,\mathrm{d}t \tag{2.73}$$

The average backscattering in a given pixel can be obtained introducing the expression of the SAR impulse response given by Eq. (2.31) within the Eq. (2.72) and integrating for the complete space, hence

$$\sigma = \int_{-\infty}^{\infty}\int_{-\infty}^{\infty} |H(f_x,f_r)|^2\,\sigma^0\,\mathrm{d}f_x\,\mathrm{d}f_r = \sigma^0\delta_x\delta_r. \tag{2.74}$$

Therefore, the value of any SAR image pixel has been divided in two contributions. First, the pixel will contain a deterministic-like RCS value (σ) proportional to the average backscattering coefficient (weighted by the resolution cell dimensions), Eq. (2.74). Second, the pixel value will contain a random contribution, which is the speckle, governed by $\mathcal{N}_c(0,\sigma^2/2)$ and characterized by the autocorrelation function given by Eq. (2.71).

2.1.6 SAR Speckle Multiplicative Noise Model

The value of each SAR image pixel has been divided into two contributions: a deterministic-like RCS value, which corresponds to the incoherent power of the area under study, modulating a random stationary speckle process. It is important to clarify that the speckle noise is not a random process, it is a true electromagnetic measurement. Despite this deterministic nature, the speckle value can not be predicted due to its complexity, fact that in turn allows the speckle to be interpreted as a noise-like process which degrades the deterministic component σ.

To assume the speckle as a noise process allows to define a noise model for the speckle and the deterministic signal component. Given the exponential pdf of the intensity image, Eq. (2.60), and introducing the change of variable $I = \sigma^2 z$, the following distribution is obtained

$$p_z(z) = \exp(-z) \qquad z \in [0,\infty) \tag{2.75}$$

The previous equation states that the value of the pixel intensity can be regarded as a deterministic value, containing information about the incoherent scattered power, multiplied by a unit mean exponentially distributed speckle noise. This is the reason why many times speckle is referred as intensity multiplicative noise component [3,8,12,75]. The phase of a SAR image, as it has been shown in Section 2.1.4, is uniformly distributed. Hence, it makes no sense to introduce a deterministic phase term in the formulation of the complex reflectivity, as it would be completely randomized by the uniform probability density function of the phase component.

As a consequence, the SAR image $S(x,r)$ can be described by the following noise model

$$S(x,r) = \sqrt{\sigma^0}n\exp(j\theta) \tag{2.76}$$

where n denotes the multiplicative speckle component in amplitude, characterized by $E\{n\} = 1$ and $\mathrm{var}\{n\} = 1$ and θ is the additive component of speckle in phase uniformly distributed. The component bearing the useful information σ is independent from the noise term $n\exp(j\theta)$.

The speckle multiplicative noise model is only valid when the amplitude or the intensity of a SAR image is considered. Due to the uniformity of the speckle phase noise, this model can not be further employed for multidimensional SAR imagery.

2.2 SAR Interferometry

Up to this point, interest has been concerned with the formation and the properties of single SAR images. The main feature of a SAR system, in front of conventional radar systems, is the azimuth resolution

increase on the basis of carrying out a recording of complex data, as well as a coherent processing of such a data. As it has been made evident in the previous section, despite the SAR images complex nature, its phase does not carry information at all. On the other hand, SAR images are contaminated by speckle, a noise-like signal, although it is a true electromagnetic measurement.

In this section, interest will be focused on combining different SAR images leading to multichannel or multidimensional SAR imagery. Any change in the sensor's geometry, in the operating frequency, in the employed polarization or in the reflectivity scene will produce a change within the SAR image. In those cases in which the changes give rise to correlated images, the phase difference between the SAR images will contain useful information. When SAR images are completely correlated, each of the individual images is contaminated by speckle, but the phase relation between them will contain useful information free of degrading factors.

There exist two main types of multidimensional SAR imagery: SAR Interferometry (InSAR) [76] and SAR Polarimetry (PolSAR) [77]. The combination of these two data types, which is called Polarimetric SAR Interferometry (PolInSAR) [42], is based on combining the advantages of each technique. This section will be focused specially in InSAR, whereas PolSAR and PolInSAR will be considered later. Despite being out of the scope of this work, there exist another way to combine different SAR images called differential interferometry (DinSAR) [78]. In this case, SAR images are combined in order to show up topographic changes.

SAR Interferometry is basically based on the creation of an interferogram by using two complex SAR images of the same area, but acquired from slightly different positions. Therefore, the imaging geometry changes from the first SAR image to the second one. This change produces the phase difference between both SAR images to contain information about the scene's topography. This system configuration is also called *Across-Track* interferometry, in contrast with *Along-Track* interferometry [79, 80]. The two complex SAR images can be acquired either, simultaneously using two antennas in the same platform (single-pass interferometry), or sing the same system in repeated passes over the same scene (repeat-pass interferometry [44, 45]). In the later case, the phase difference between both SAR images will also depend on possible scatterer variations between the different passes.

2.2.1 SAR Interferometry Geometric Approach

In this section, a geometric approach for SAR interferometry is presented. The use of this approach makes possible to see the relationship between the surface and the sensor geometries in order to obtain the information contained within the SAR images phase difference. This approach is based on several simplifications as to consider a flat Earth or not considering signal spectral properties. Hence, the approximation is not valid for satellite geometries with large swaths or for airborne geometries. Detailed developments on SAR interferometry can be found in [14, 76, 81, 82, 83].

The interferometric SAR system is based on the geometry shown by Fig. 2.8. Each of the SAR platforms, denoted by T_1 and T_2 respectively, acquires a SAR image as it has been explained in Section 2.1. The two antennas are separated by a given baseline B, observing the same point P at range r from the first platform and at range $r + \Delta r$ from the second one. For the geometric approach, the observed point P will be assumed to be a point scatterer characterized by Eq. (2.10). Therefore, the two SAR images are

$$S_1(x_1, r_1) = |S_1(x_1, r_1)| \exp(j\theta_1(x_1, r_1)) \tag{2.77}$$

$$S_2(x_2, r_2) = |S_2(x_2, r_2)| \exp(j\theta_2(x_2, r_2)). \tag{2.78}$$

Both SAR images observe the reflectivity scene from two different locations. Therefore, a given pixel of the first SAR image does not correspond to the same reflectivity contained in the pixel of the second image. There exist several techniques developed to solve this problem, known as image co-registering.

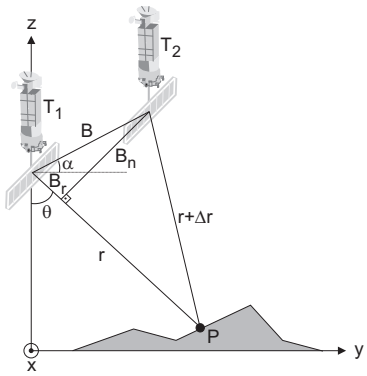

Figure 2.8: Interferometric SAR system geometry.

In a classical approach, both images are registered, with a pixel accuracy, by using cross correlation techniques. In many cases, these techniques are not enough to obtain quality interferograms. To fulfill the quality requirements, sub-pixel registration techniques are employed [19, 84]. Once the SAR image pixels refer to the same area, the complex interferogram is defined as

$$S_1(x_1, r_1)S_2^*(x_2, r_2) = |S_1(x_1, r_1)|\,|S_2(x_2, r_2)| \exp(j(\theta_1(x_1, r_1) - \theta_2(x_2, r_2))). \tag{2.79}$$

Owing to the fact that both SAR images observe the same point scatterer P from slightly different positions, the phase of each SAR image can be written, taking into account the geometry depicted by Fig. 2.8, as

$$\theta_1(x_1, r_1) = -j\frac{4\pi}{\lambda}r + \theta_{s1} \tag{2.80}$$

$$\theta_2(x_1, r_1) = -j\frac{4\pi}{\lambda}(r + \Delta r) + \theta_{s2}. \tag{2.81}$$

Assuming that the phases due to the scatterer, θ_{s1} and θ_{s2}, are equal, the interferometric phase (i.e., the phase difference) is a very sensitive measure for the range difference

$$\Delta\phi = \theta_2 - \theta_1 = \frac{4\pi}{\lambda}\Delta r \tag{2.82}$$

Owing to the circular nature of any phase measurement, the interferometric phase given by Eq. (2.82) is ambiguous within integer multiples of 2π. The removal of this ambiguity, i.e., the estimation of the absolute phase will be addressed later in this section.

To derive the information content in $\Delta\phi$, it is necessary to see the dependence of Δr on the different parameters of the imaging geometry given by Fig. 2.8. Assuming this geometry

$$(r + \Delta r)^2 = (r - B_r)^2 + B_n^2 \tag{2.83}$$

where

$$B_n = B\cos(\theta - \alpha) \tag{2.84}$$

$$B_r = B\sin(\theta - \alpha). \tag{2.85}$$

B_r is called the parallel baseline, whereas B_n is the perpendicular baseline. In a spaceborne SAR system, the contribution of the term Δr^2 can be neglected in front of the parameter r. Therefore, Δr can be simplified as

$$\Delta r = \frac{B^2}{2r} + B\sin(\theta - \alpha). \tag{2.86}$$

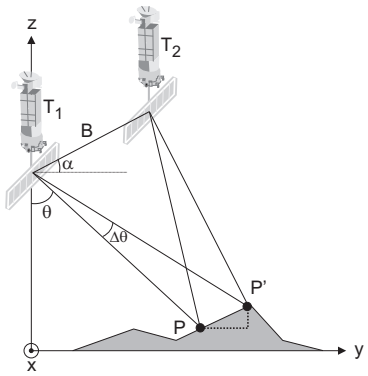

Figure 2.9: InSAR geometry.

The geometric approach for InSAR is based on a spaceborne system. In such a case, the difference between the baseline B and the range r is about several orders of magnitude, allowing to neglect the first addend in Eq. (2.86). Hence, Δr can be approximated by

$$\Delta r \approx B \sin(\theta - \alpha). \tag{2.87}$$

With the previous approximation, the phase difference $\Delta\phi$, can be written as

$$\Delta\phi \approx \frac{4\pi}{\lambda} B \sin(\theta - \alpha). \tag{2.88}$$

Eq. (2.88) corresponds to the phase of a single pixel in the interferogram. However, this phase is not useful as the wavelength is so short that the phase is wrapped, apart from the fact that it also contains range information. Due to this ambiguity, the phase difference between two adjacent pixels, P and P' will be studied in the following

$$\Delta\left(\Delta\phi\right) = \frac{4\pi}{\lambda}\Delta\left(\Delta r\right). \tag{2.89}$$

Fig. 2.9 shows the geometry to obtain $\Delta\left(\Delta\phi\right)$. The viewing geometry changes form the pixel P to P', introducing a variation in the range Δr as well as a change in the viewing angle by a factor $\Delta\theta$. Hence, the phase difference between both pixels can be written, using Eq. (2.88), as

$$\Delta\left(\Delta\phi\right) = \frac{4\pi}{\lambda}\left[B\sin(\theta - \alpha) - B\sin(\theta + \Delta\theta - \alpha)\right]. \tag{2.90}$$

As the angle difference $\Delta\theta$ is small, it can be neglected compared with the term $\theta - \alpha$. Likewise, the small angle approximation can be used for the sine function, $\sin\left(\Delta\theta\right) \approx \Delta\theta$. On the basis of these approximations, the phase difference between two pixels, Eq. (2.90), becomes

$$\Delta\left(\Delta\phi\right) = \frac{4\pi}{\lambda}\Delta\theta B\cos\left(\theta - \alpha\right) = \frac{4\pi}{\lambda}\Delta\theta B_n. \tag{2.91}$$

As it has been pointed out previously, the SAR system gathers reflectivity data referred to the slant-range coordinate system, denoted by (x, r). In order to derive the expression of the term $\Delta\phi$ it is very important to take into account this geometry. The derivation of $\Delta\phi$ will be divided into two components

$$\Delta\left(\Delta\phi\right) = \Delta\left(\Delta\phi\right)_{flat} + \Delta\left(\Delta\phi\right)_{topography}. \tag{2.92}$$

The fist component is devoted to take into account the range difference between both pixels, whereas the second one accounts for the height difference projected into the slant-range coordinate system.

First of all, it will be assumed that both pixels, P and P', lie at the same height. Assuming that the difference in the viewing angle $\Delta\theta$ is small, it is possible to obtain the approximation $r\sin(\Delta\theta) \approx r\Delta\theta = \Delta r/\tan(\theta)$, allowing to write the phase difference, $\Delta\left(\Delta\phi\right)_{flat}$, in the following way

$$\Delta\left(\Delta\phi\right)_{flat} = \frac{4\pi}{\lambda}\frac{B_n}{r}\frac{\Delta r}{\tan(\theta)}. \tag{2.93}$$

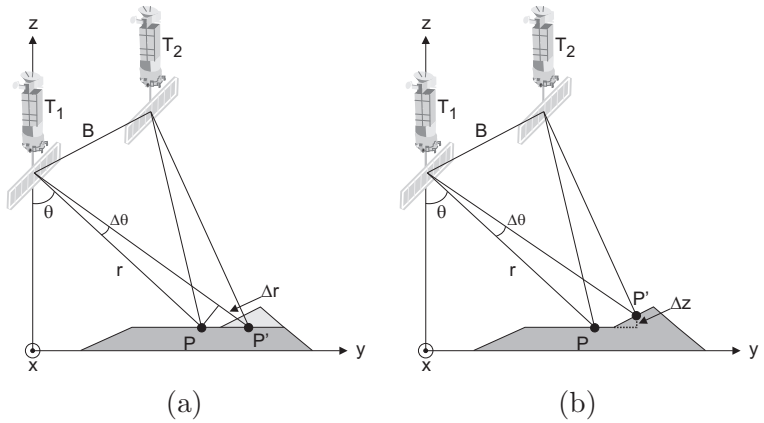

Figure 2.10: InSAR geometry.

The previous equation states that a flat earth generates a linear interferometric phase pattern, called Flat Earth Component. Therefore, if the goal is to obtain a phase term proportional to the scene topography, the flat earth component must be removed from the interferometric phase.

The second component is $\Delta\left(\Delta\phi\right)_{topography}$. In this case, the pixels P and P' will be assumed to lie at the same range r, but located at a different position in the z axis, see Fig. 2.10. In this case, the phase difference term will only account for the phase difference induced by the topography. As in the previous case, the phase difference $\Delta\theta$ is assumed small enough to apply the small phase approximation for the sine function, $r\sin(\Delta\theta) \approx r\Delta\theta = \Delta z/\sin(\theta)$. Finally, the phase difference term proportional to the topography in Eq. (2.92) is

$$\Delta\left(\Delta\phi\right)_{topography} = \frac{4\pi}{\lambda}\frac{B_n}{r}\frac{\Delta z}{\sin(\theta)}. \tag{2.94}$$

The use of the previous equation in order to retrieve the topographic information from the scene under observation has to be done taking into account two points. First of all, Eq. (2.94) is only valid for the absolute phase difference, and not for a wrapped version of it. Hence, the difference phase obtained from the interferogram has to be unwrapped in order to obtain a height absolute value [85]. Second, the topographic phase information, Eq. (2.94), is not an absolute height measurement as it only gives height differences between adjacent pixels. This makes necessary the knowledge about the absolute height, at least in one pixel, in order to refer the rest of the phase image to this pixel.

The topographic interferometric phase given by Eq. (2.94), which is derived from the interferogram, Eq. (2.79), is a wrapped phase difference, that is, only values in the range $[-\pi, \pi)$ are known, whereas the integer number of cycles is unknown. In a wrapped interferometric phase image, the phase period between $-\pi$ and π is known as fringe. As a result, it can be known which is the height information encoded in a 2π cycle of phase, called height ambiguity

$$\Delta h_{2\pi} = \frac{\lambda\sin(\theta)r}{2B_n}. \tag{2.95}$$

The height ambiguity given by Eq. (2.95) depends mainly on the wavelength λ and the normal baseline B_n. In order to extract some conclusions about the best parameters to obtain the interferogram, it is valuable to derive the height sensitivity

$$\frac{\partial(\Delta\left(\Delta\theta\right))}{\partial\left(\Delta h\right)} = \frac{4\pi}{\lambda}\frac{B_n}{r\sin(\theta)}. \tag{2.96}$$

As Eq. (2.96) states, the height sensitivity is high for large normal baselines and decreases with large wavelengths. The baseline cannot be increased arbitrarily, as the correlation between the pair of SAR images would decrease, whose effect, called baseline decorrelation, would be to increase phase noise [86].

2.2.2 Interferometric SAR System Model

In the previous section, assuming a simplified SAR system geometry, as well as deterministic scatterers, it has been shown that the interferometric phase can be related with the topography of the scene under observation. Since most of the targets observed by a SAR system are distributed scatterers, it is necessary to increase the complexity of the interferometric SAR system model in order to derive the response of such a system to this type of scatterers.

A distributed scatterer has been defined within Section 2.1.5 as a set of randomly located point scatterers, characterized by the average scattering coefficient σ^0 for two-dimensional scatters, or by the volume scattering coefficient σ_v for volume scatterers. The former one can be assumed as a particular case of the volume scattering coefficient. From now, a scattering volume will be assumed. In this case, the volume scattering is characterized by the autocorrelation function

$$R_{\widetilde{u}}\left(\overrightarrow{r},\overrightarrow{r}'\right)=E\left\{\widetilde{u}(\overrightarrow{r})\widetilde{u}^*(\overrightarrow{r}')\right\}=\sigma_v\left(\overrightarrow{r}\right)\delta\left(\overrightarrow{r}-\overrightarrow{r}'\right) \tag{2.97}$$

where $\overrightarrow{r}$ represents the location vector $[x,y,z]^T$ and $\widetilde{u}(\overrightarrow{r})=\widetilde{u}(x,y,z)$ denotes the random volume reflectivity function. $\delta(\overrightarrow{r})$ denotes the Dirac's delta function in the space.

Since in this case, the reflectivity function has a random component, interest is focused on the average interferometric response, instead of the interferometric phase response for a particular pixel. Hence, taking into account the two complex SAR images $S_1(x_1,r_1)$ and $S_2(x_2,r_2)$, the average interferometric response is given by

$$E\left\{S_1(x_1,r_1)S_2^*(x_2,r_2)\right\}. \tag{2.98}$$

Apart from the autocorrelation function given by Eq. (2.97), it may happen the scattering to change between the two acquisitions. This effect can be very clear with repeat-pass interferometry. In this case, it is assumed that the scatterer autocorrelation function is given by

$$R_{\widetilde{u}_1\widetilde{u}_2}\left(\overrightarrow{r}_1,\overrightarrow{r}_2\right)=E\left\{\widetilde{u}_1(\overrightarrow{r}_1)\widetilde{u}_2^*(\overrightarrow{r}_2)\right\}=\sigma_{ve}\left(\overrightarrow{r}_1\right)\delta\left(\overrightarrow{r}_1-\overrightarrow{r}_2\right) \tag{2.99}$$

where $\sigma_{ve}(\overrightarrow{r})$ is the volume scattering coefficient of scatterers common to both images [87, 88]. It can be interpreted as the temporarily stable scattering contribution; those contributions changing between observations are cancelled in the average process.

Within Section 2.1.3, it was found which is the SAR system response to a distributed scatterer. Before to derive the average interferometric response, it has to be taken into account that the two SAR images, $S_1(x_1,r_1)$ and $S_2(x_2,r_2)$, are taken from slightly different look angles. Therefore, the system coordinates, under which each of the SAR images are defined, are different. However, the difference in look angle $\Delta\theta=\theta_1-\theta_2\simeq B_n/r$ is small enough that a single coordinate system (x,r) oriented at $\theta=(\theta_1-\theta_2)/2$ can be considered. This consideration can not be taken in the term $\exp(-j2\overrightarrow{k}\cdot\overrightarrow{r}'_s)$, as it requires the distinction between the two wavevectors $\overrightarrow{k}_1$ and $\overrightarrow{k}_2$. Using Eq. (2.37), the response for each of the SAR images are

$$S_1(x_1,r_1)=\exp(-j2k_1r_1)\int_{V'}\widetilde{u}(x',y',z')\exp(-j2\overrightarrow{k}_1\cdot\overrightarrow{r}')h_1(x_1-x',r_1-r')\,\mathrm{d}V' \tag{2.100}$$

$$S_2(x_2,r_2)=\exp(-j2k_2r_2)\int_{V'}\widetilde{u}(x',y',z')\exp(-j2\overrightarrow{k}_2\cdot\overrightarrow{r}')h_2(x_2-x',r_2-r')\,\mathrm{d}V'. \tag{2.101}$$

As it has been performed in the previous section, the first step to obtain the interferogram is to register the pair of SAR images. The registration forces the azimuth coordinates to be $x=x_1=x_2$, whereas it forces the range coordinate to be $r_2=r_1-B_r$. After registering the SAR image $S_2(x_2,r_2)$ to $S_1(x_1,r_1)$, Eqs. (2.100) and (2.101) are

$$S_1(x,r_1)=\exp(-j2k_1r_1)\int_{V'}\widetilde{u}(x',y',z')\exp(-j2\overrightarrow{k}_1\cdot\overrightarrow{r}')h_1(x-x',r_1-r')\,\mathrm{d}V' \tag{2.102}$$

$$S_2(x,r_2) = \exp(-j2k_2r_2)\int_{V'}\widetilde{u}(x',y',z')\exp(-j2\overrightarrow{k}_2\cdot\overrightarrow{r}')h_2(x-x',r_2-r')\,\mathrm{d}V'. \tag{2.103}$$

In the previous equations, it has been considered that each of the SAR images have been derived with a different SAR system response, h_1 and h_2 respectively. SAR system conditions may change between acquisitions, but without loss of generality, it can be assumed that $h = h_1 = h_2$. Therefore, assuming a distributed scatterer defined by (2.99), the average interferometric response may be written as

$$\begin{aligned} E\{S_1(x,r_1)S_2^*(x,r_2)\} &= \exp(-j2(k_1r_1-k_2r_2))\int_{V'}\sigma_{ve}(\overrightarrow{r}')\exp(-j2(\overrightarrow{k}_1-\overrightarrow{k}_2)\cdot\overrightarrow{r}') \\ &\cdot\ h_1(x-x',r_1-r')h_2^*(x-x',r_2-r')\,\mathrm{d}V' \\ &= \exp(-j2(k_1r_1-k_2r_2)) \\ &\cdot\ \int_{V'}\sigma_{ve}(\overrightarrow{r}')\exp(-j2(\overrightarrow{k}_1-\overrightarrow{k}_2)\cdot\overrightarrow{r}')|h_1(x-x',r_1-r')|^2\,\mathrm{d}V'. \end{aligned} \tag{2.104}$$

The first term $\exp(-j2(k_1r_1-k_2r_2))$ is the deterministic component of the interferometric phase containing the information about the topography, as developed within Section 2.2.1, Eqs. (2.86) and (2.87). The integral component within Eq. (2.104) produces the interferogram to be random as a consequence of the scatterer randomness. In the same way as it has been shown for single SAR images, the data randomness produces a degradation of the useful information; in this case, the topographic height information.

2.2.3 Interferometric SAR Data Statistics

Within Sections 2.1.4 and 2.1.5 a statistical model for single SAR images was introduced. Assuming a distributed scatterer as a set of randomly located point scatterers, characterized by an average volume scattering coefficient σ_v, SAR images can be assumed to be described as $\mathcal{N}_c(0,\sigma^2/2)$. This model represents an idealization of the reality which offers the possibility to work with a relatively simple model. This model will be used as a starting point to derive the statistical description for InSAR data.

As mentioned within preceding sections, InSAR is based on the interaction between two SAR images of the same scene, in which the acquisition geometry has changed. First, a two-dimensional complex scatterer vector, containing both SAR images, is defined as

$$\mathbf{k} = [\ S_1\ S_2\ ]^T. \tag{2.105}$$

As is has been presented within Section 2.1.4, S_1 and S_2 are described by zero-mean, complex, Gaussian pdfs, $\mathcal{N}_c(0,\sigma^2/2)$. Therefore, $\mathbf{k}$ can be assumed to be described by a bivariate, zero-mean, complex, Gaussian pdf [89, 21, 7, 72, 22] $\mathcal{N}(\mathbf{0},[C])$

$$p_{\mathbf{k}}(\mathbf{k}) = \frac{1}{\pi^2|[C]|}\exp(-\mathbf{k}^{*T}[C]^{-1}\mathbf{k}) \tag{2.106}$$

where ^{*T} denotes the transpose complex conjugate. The previous distribution is completely characterized by the 2 by 2 complex covariance matrix $[C]$, which in this case is defined as

$$[C] = E\{\mathbf{k}\mathbf{k}^{*T}\} = \begin{bmatrix} \sigma_1 & \psi\rho \\ \psi\rho^* & \sigma_2 \end{bmatrix}. \tag{2.107}$$

The parameter σ_k is defined as the backscattering coefficient in the kth image, $E\{|S_k|^2\}$, whereas $\psi = \sqrt{\sigma_1\sigma_2}$ represents a measure of the average power in the two channels. The parameter ρ is the correlation coefficient between both SAR images

$$\rho = |\rho|\exp(j\phi_x) = \frac{E\{S_1S_2^*\}}{\sqrt{E\{|S_1|^2\}E\{|S_2|^2\}}} = \frac{E\{S_1S_2^*\}}{\sqrt{\sigma_1\sigma_2}}. \tag{2.108}$$

The correlation coefficient absolute value is simply called coherence. There is no a clear agreement about the symbol representing the correlation coefficient. Some authors denote it with the symbol γ for the particular case of InSAR. The symbol ρ is mainly employed to describe PolSAR data. In this text, in order to describe the correlation properties in the most general way, the symbol ρ has been chosen to describe the correlation coefficient for InSAR data, as well as for PolSAR data. The diagonal terms of the covariance matrix refer to the intensity properties of each of the complex SAR images. The first-order statistics of these terms have been studied within Section 2.1.4. Thus, attention will now be confined to the properties of the covariance matrix off-diagonal terms $S_1 S_2^* = r_1 r_2 \exp(j(\theta_1 - \theta_2))$. If the amplitude is denoted by $z = r_1 r_2$ and the phase $\phi = \theta_1 - \theta_2$, the joint pdf for the amplitude and phase is [22]

$$p_{z,\phi}(z,\phi) = \frac{2z}{\pi\psi^2(1-|\rho|^2)} \exp\left(\frac{2|\rho|z\cos(\phi-\phi_x)}{\psi(1-|\rho|^2)}\right) K_0\left(\frac{2z}{\psi(1-|\rho|^2)}\right) \tag{2.109}$$

where $K_0(z)$ is the modified Bessel function of the third kind. The phase distribution can be obtained integrating out the amplitude variable z. Therefore the phase pdf is [5, 21, 90, 20, 22, 91]

$$p_\phi(\phi) = \frac{(1-|\rho|^2)}{2\pi}\left\{\frac{\beta(\frac{1}{2}\pi + \arcsin(\beta))}{(1-\beta^2)^{3/2}} + \frac{1}{1-\beta^2}\right\} \qquad \phi \in [-\pi, \pi) \tag{2.110}$$

where $\beta = |\rho|\cos(\phi - \phi_x)$. The phase difference distribution $p_\phi(\phi)$ is unimodal, symmetric and modulus 2π about its mode, which occurs at ϕ_x. As Eq. (2.110) shows, the phase difference distribution only depends on the coherence $|\rho|$. For a coherence close to 1, the distribution resembles a delta function located at ϕ_x, whereas for a coherence close to zero, the distribution is very close to a uniform distribution. Fig. 2.11 shows this behavior. The fist conclusion which can be extracted from this behavior is that the phase difference ϕ appears noisy for low coherences. For the extreme case in which the coherence is zero, the phase difference does not contain useful information.

An important point that has to be taken into consideration with respect to the phase difference distribution is the circular nature of the phase. The phase difference given by the argument of the interferogram, Eq. (2.79), is only a value within the interval $[-\pi, \pi)$. Thus, this behavior has to be carefully considered when the phase difference distribution is employed. If the distribution given by Eq. (2.110) is considered in a 2π interval about ϕ_x, the mean and variance values have the expressions [7, 22]

$$E\{\phi\} = \phi_x \tag{2.111}$$

$$\mathrm{var}\{\phi\} = \frac{\pi^2}{3} - \pi\arcsin(|\rho|) + \arcsin^2(|\rho|) - \frac{1}{2}\mathrm{Li}_2(|\rho|^2) \tag{2.112}$$

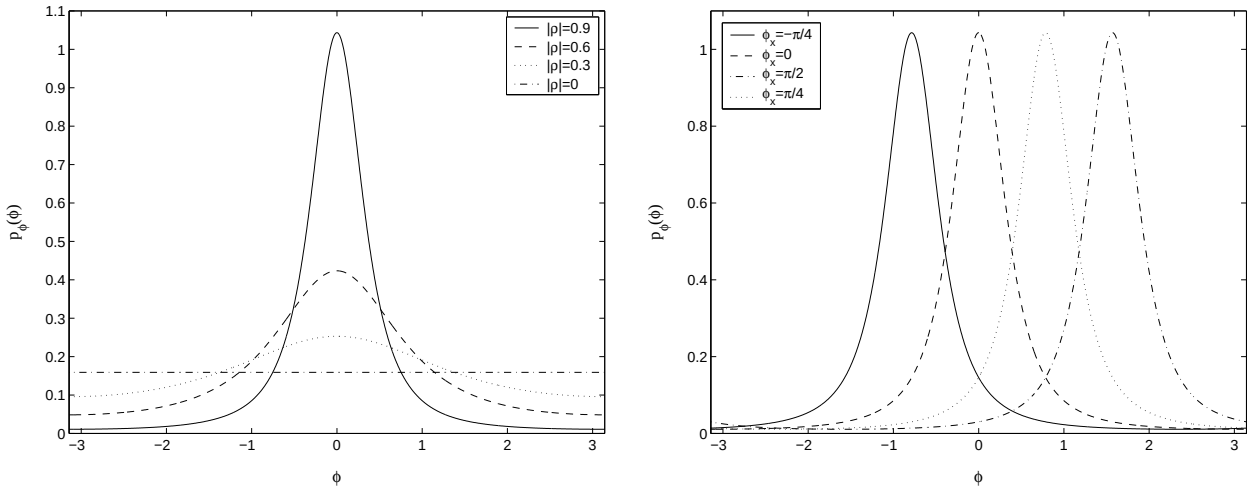

(a) (b)

Figure 2.11: Interferometric phase statistics. (a) Effect of coherence $|\rho|$. (b) Effect of ϕ_x for $|\rho| = 0.9$.

where $\mathrm{Li}_2(\cdot)$ denotes the Euler's dilogarithm. On the contrary, if the phase difference pdf is assumed to lie in the interval $[-\pi, \pi)$, the mean and variance values take the form [7, 22]

$$E\{\phi\} = \phi_x + \frac{|\rho|\sin(\phi_x)}{\sqrt{1-|\rho|^2\cos^2(\phi_x)}}\arccos(|\rho|\cos(\phi_x)) \tag{2.113}$$

$$\begin{aligned}\mathrm{var}\{\phi\} &= \frac{1-|\rho|^2}{1-|\rho|^2\cos^2(\phi_x)}\left\{\frac{\pi^2}{4} - \pi\arcsin(|\rho|\cos(\phi_x)) + (\arcsin(|\rho|\cos(\phi_x)))^2\right\} \\ &+ \frac{1}{2}\sum_{n=1}^{\infty}\frac{1-|\rho|^{2n}}{n^2}.\end{aligned} \tag{2.114}$$

Therefore, when the phase difference is assumed as a wrapped measurement in the interval $[-\pi, \pi)$, to describe the statistics in terms of the mean and the variance fails in order to obtain the useful information ϕ_x. This handicap can be overcome if the mean and the variance are calculated using unwrapped data. At the same time, this fact presents the problem that phase unwrapping can be incorrect due to the presence of phase residues [85]. As it will be shown later, this fact has important consequences when phase noise has to be reduced. The other possible way to overcome this problem, is to analyze the problem in the complex plane.

2.2.4 Interferometric SAR Coherence

It has been shown that the phase pdf is governed by the coherence $|\rho|$, as shown by Eq. (2.110). The coherence $|\rho|$ can be expressed in terms of the scatterer properties, as well as the system properties. Without loss of generality, it can be assumed that $x = 0$ and $r = 0$ in Eq. (2.104). First, for each of the complex SAR images, the signal intensities are

$$I_1 = E\{S_1 S_1^*\} = \int_{V'} \sigma_{v_{S1}} |h(-x', -r_1')|^2 \, \mathrm{d}V' \tag{2.115}$$

$$I_2 = E\{S_2 S_2^*\} = \int_{V'} \sigma_{v_{S2}} |h(-x', -r_2')|^2 \, \mathrm{d}V'. \tag{2.116}$$

For the sake of simplicity, it can be assumed that both intensities are equal, that is, $\sigma_v = \sigma_{v_{S1}} = \sigma_{v_{S2}}$. To obtain a more realistic signal model, it can be assumed that each of the image intensities is also contaminated by thermal noise introduced by the SAR system components [89, 92]. The noise intensities, denoted by N_1 and N_2 respectively, are uncorrelated with the SAR images. Getting rid of the deterministic components of the phase difference, assuming a thermal noise component and introducing Eqs. (2.104), (2.115) and (2.116) to Eq. (2.108), the correlation coefficient takes the expression

$$\rho = \frac{\int_{V'} \sigma_{ve}(\overrightarrow{r}') \exp(-j2(\overrightarrow{k}_1 - \overrightarrow{k}_2)\cdot\overrightarrow{r}')|h(x-x', r_1-r')|^2 \, \mathrm{d}V'}{\int_{V'} \sigma_v |h(-x', -r')|^2 \, \mathrm{d}V' + N}. \tag{2.117}$$

The correlation coefficient ρ can be decomposed as the product of different contributions [89, 92]. Each of these components contributes with a magnitude less or equal than 1. Therefore, in order to reduce the noise content within the phase difference it is mandatory to reduce, or even, to eliminate each one of these effects. In [92], the correlation coefficient was decomposed in three dominant terms. The expressions of each of these terms are:

- The first term takes into account the decorrelation introduced by the thermal additive noises. In this case

$$\rho_{SNR} = \frac{\int_{V'} \sigma_v(\overrightarrow{r}')|h(-x', -r')|^2 \, \mathrm{d}V'}{\int_{V'} \sigma_v(\overrightarrow{r}')|h(-x', -r')|^2 \, \mathrm{d}V' + N} = \frac{1}{1 + \frac{1}{SNR}}. \tag{2.118}$$

  When the noise power is zero, there is no decorrelation due to thermal noise, therefore, $\rho_{SNR} = 1$. On the contrary the lower the signal to noise ration (SNR), the higher the decorrelation and the higher the phase noise content.

· As mentioned previously, the scatterer features may change between the pair of SAR acquisitions. In Eq. (2.99), the term σ_{ve} accounts for the common scattering mechanisms between acquisitions. Therefore

$$\rho_{temporal} = \frac{\int_{V'} \sigma_{ve}(\overrightarrow{r}')|h(-x',-r')|^2\,\mathrm{d}V'}{\int_{V'} \sigma_{v}(\overrightarrow{r}')|h(-x',-r')|^2\,\mathrm{d}V'}. \tag{2.119}$$

For those situations in which there is no variation on the scattering mechanism between the pair of acquisitions, i.e., $\sigma_v = \sigma_{ve}$, $\rho_{temporal} = 1$. On the contrary, if there is no common scattering mechanisms between acquisitions $\rho_{temporal} = 0$.

· The third term has a crucial importance in SAR interferometry. This term takes into account the fact that the two SAR images are taken from slightly different look angles.

$$\rho_{spatial} = \frac{\int_{V'} \sigma_{ve}(\overrightarrow{r}')\exp(-j2(\overrightarrow{k}_1 - \overrightarrow{k}_2)\cdot\overrightarrow{r}')|h(-x',-r')|^2\,\mathrm{d}V'}{\int_{V'} \sigma_{ve}(\overrightarrow{r}')|h(-x',-r')|^2\,\mathrm{d}V'}. \tag{2.120}$$

This term has its origin in the fact that due to the difference in the look angle, the coherent addition from the echoes due to the individual scatterers varies. It should be mentioned that this term is inherent to InSAR. It is easy to see that the effect of this term can be removed making $\overrightarrow{k}_1 = \overrightarrow{k}_2$, but then, no information about surface's topography would be available as both SAR images would contain exactly the same information.

The term $\rho_{spatial}$ can be better understood if a simplification is applied to the term $(\overrightarrow{k}_1 - \overrightarrow{k}_2)\cdot\overrightarrow{r}'$. Assuming $\Delta k = k_1 - k_2$, which makes possible to define $k_1 = k + \Delta k/2$ and $k_2 = k - \Delta k/2$ and the difference in the look angle to be $\Delta\theta \simeq \sin(\Delta\theta) = B_n/r$, allows to rewrite the phase term accounting for the difference in look angle as

$$\begin{aligned} & \exp(-j2(\overrightarrow{k}_1 - \overrightarrow{k}_2)\cdot\overrightarrow{r}') \\ = \; & \exp\left(-j2\left\{\left(\frac{k\cos(\theta)B_n}{r} + \Delta k\sin(\theta)\right)y' + \left(\frac{k\sin(\theta)B_n}{r} + \Delta k\cos(\theta)\right)z'\right\}\right). \end{aligned} \tag{2.121}$$

The previous equation shows that $\rho_{spatial}$ can be further split into two new terms. The first term has the following expression

$$\rho_{range} = \frac{\int \sigma_{ve}(\overrightarrow{r}')\exp(-j2(\frac{k\cos(\theta)B_n}{r} + \Delta k\sin(\theta))y')|h(-x',-r')|^2\,\mathrm{d}x'\,\mathrm{d}y'}{\int |h(-x',-r')|^2\,\mathrm{d}x'\,\mathrm{d}y'}. \tag{2.122}$$

This contribution can be reduced making $\Delta k = -(kB_n)/(r\tan(\theta))$. The first option to make $\rho_{range} = 1$ is to allow a central frequency change of the SAR system in each of the SAR surveys. Such a configuration is known as a tunable SAR system [86]. For practical purposes, the variation in the look angle generates a shift and a stretch of the imaged terrain spectra [86, 93]. However, if the relative system bandwidth is small, the stretch can be neglected, and only a frequency shift can be assumed [86, 93]. As a consequence, the decorrelation induced by the difference in look angle can be removed if those non-common spectral bandwidth are filtered out. This process is called Wavenumber Shift Filtering [86]. The second contribution can be rewritten as

$$\rho_{volume} = \frac{\int_{z'} \sigma_{ve}(z')\exp(-j2(\frac{k\sin(\theta)B_n}{r} + \Delta k\cos(\theta))z')\,\mathrm{d}z'}{\int_{z'} \sigma_{ve}(z')\,\mathrm{d}z'}. \tag{2.123}$$

This term accounts for the decorrelation induced by a finite distributed scatterers in the z dimension [86]. Through the use of ρ_{volume}, it is possible to derive information about the scatterer's structure in the z dimension [42].

As it has been developed in the previous paragraphs, the coherence information can be split in four dominant terms into the following way

$$\rho = \rho_{SNR}\,\rho_{temporal}\,\rho_{spatial} = \rho_{SNR}\,\rho_{temporal}\,\rho_{range}\,\rho_{volume}. \tag{2.124}$$

The first term is purely due to the SAR system, whereas the rest of the terms are due to the scatter's nature. Hence, the terms due to the scatterer are affected by any change within the SAR system that produces to gather information in a different way. For example, these decorrelation terms are affected by the wave polarization.

Apart from the decorrelation effects mentioned here. It is possible to define other different decorrelation sources. In this case, these are due to incorrect processing of the SAR images or incorrect interferogram formation. A clear example is the registration step, as an incorrect image co-registering introduces decorrelation effects between the pair of SAR images.

2.2.5 Phase Difference Noise Model

As it has been presented throughout this section, InSAR is based on the information contained in the interferometric phase, Eq. (2.79), which is calculated as the complex Hermitian product phase of a pair of SAR images. As it has been explained within Section 2.1.6, the multiplicative speckle noise model can not be employed to study the speckle noise effects over the phase difference, as the phase for each of the SAR images is modelled as a uniform distribution within the interval $[-\pi, \pi)$, eliminating any useful information.

The distribution of the phase difference, see Eq. (2.110), has its mode at ϕ_x. If the phase difference is assumed to lie within the interval $[-\pi, \pi)$, the expectation, as well as the variance are clearly biased. On the other hand, if the phase difference is analyzed in the interval $[\phi_x - \pi, \phi_x + \pi)$, the expectation and the variance give more clear information. As given by Eq. (2.111), the expectation is just the distribution mode ϕ_x, which contains the topographic information. Besides, the variance gives information about the spread of the distribution around ϕ_x, i.e., it gives information about the noise content. As a result of all these facts, the phase difference can be characterized by an additive noise model within the interval $[\phi_x - \pi, \phi_x + \pi)$ [94]

$$\phi = \phi_x + v \tag{2.125}$$

where ϕ is the measured phase difference, ϕ_x is the phase without noise and v is the phase zero-mean noise with a standard deviation σ_v. The noise power σ_v^2 is given by Eq. (2.112).

The phase difference noise model has to be carefully applied. First of all, this model can only be applied over the real plane. On the other hand, this model is only valid, as mentioned, within the interval $[\phi_x - \pi, \phi_x + \pi)$. As the interferometric phase is always wrapped within $[-\pi, \pi)$, is it necessary to unwrap the phase in a neighborhood of the pixel under study in order to use the model. One of the main problems caused by phase noise are the phase residues, which hinder the unwrapping process itself.

2.3 SAR Polarimetry

This section is devoted to present the basis of SAR Polarimetry (PolSAR). Equally as it has been presented with InSAR, PolSAR represents an increase of information by acquiring more than one SAR image. Also, whenever the SAR images are correlated it will be possible to retrieve scatterer properties from the phase difference measurement.

In the case of PolSAR data, the information increase is obtained on the basis of wave polarization diversity. The main feature of a transverse electromagnetic wave is the vectorial nature of the EM field which is known as polarimetry. Therefore, combining the polarization of the illuminating wave with the antenna polarization in which the scattered wave is recorded, it is possible to increase the number of information channels. The main advantage of the polarization diversity is the possibility to derive the scatterer response to any wave polarization state from the response to a pair of orthogonal polarization states, offering the possibility to optimize, for instance, the polarization state for maximum received power.

2.3.1 Wave Polarization

The Maxwell Equations

In 1864, J.C. Maxwell established and synthesized preceding results obtained by M. Faraday, A. Ampère and K. F. Gauss about the interaction between the electric field, the magnetic field and currents, generalizing them to variable regimes in time. The Maxwell equations represent the starting point to solve electromagnetic problems as they govern the generation and propagation of electromagnetic waves, as well as the interaction of these waves with the matter. For electromagnetic sources in a non-conducting, lossless, isotropic media, the Maxwell equations can be written as

$$\nabla \cdot \overrightarrow{E}(\overrightarrow{r},t) = \frac{\rho(\overrightarrow{r},t)}{\epsilon_0\epsilon_r} \tag{2.126}$$

$$\nabla \cdot \overrightarrow{B}(\overrightarrow{r},t) = 0 \tag{2.127}$$

$$\nabla \times \overrightarrow{B}(\overrightarrow{r},t) - \epsilon_0\epsilon_r\mu_0\mu_r\frac{\partial \overrightarrow{E}(\overrightarrow{r},t)}{\partial t} = \mu_0 \overrightarrow{J}(\overrightarrow{r},t) \tag{2.128}$$

$$\nabla \times \overrightarrow{E}(\overrightarrow{r},t) = -\frac{\partial \overrightarrow{B}}{\partial t} \tag{2.129}$$

where:

- $\overrightarrow{E}$ is the electric field intensity vector.
- $\overrightarrow{B}$ is the magnetic field induction vector.
- ρ is the electric charge density.
- $\overrightarrow{J}$ is the density current vector.
- ϵ_0 is the electric permittivity in the vacuum.
- ϵ_r is the relative electric permittivity of the media.
- μ_0 is the magnetic permeability in the vacuum.
- μ_r is the relative magnetic permeability of the media.

As shown by the Maxwell equations, all the terms referring to fields, $\overrightarrow{E}$ and $\overrightarrow{B}$, as well as the sources terms, ρ and $\overrightarrow{J}$, are defined for any time t and for any space point $\overrightarrow{r}$, which depends on the specific coordinate system. A deeper treatment about Maxwell equations can be found in [95, 96].

Wave Equation

A fundamental aspect of the Maxwell equations for the electromagnetic field is the existence of solutions consisting in progressive waves which represent the energy transport form one point to another [95, 96]. In the absence of sources, the fields which are solution of the Maxwell equations, also satisfy the wave equation

$$\nabla^2\Psi - \frac{1}{v^2}\frac{\partial^2\Psi}{\partial t^2} = 0 \tag{2.130}$$

where Ψ represents the fields $\overrightarrow{E}(\overrightarrow{r},t)$ or $\overrightarrow{B}(\overrightarrow{r},t)$. The velocity v, which is a characteristic constant of the media, is defined as

$$v = \frac{1}{\sqrt{\epsilon_0\epsilon_r\mu_0\mu_r}} = \frac{c}{\sqrt{\epsilon_r\mu_r}} \tag{2.131}$$

where c represents the speed of light in the vacuum.

As presented within the previous section, the electromagnetic fields have a time dependence. For a sinusoidal time dependence, it is said that the electric field is time-harmonic or monochromatic

$$\overrightarrow{E}(\overrightarrow{r},t) = \overrightarrow{E}_0(\overrightarrow{r})\cos(\omega t + \varphi(\overrightarrow{r})) \tag{2.132}$$

where $w = 2\pi f$ is the angular frequency in rad/s. $\overrightarrow{E}_0(\overrightarrow{r})$ is the real electric field amplitude, whereas $\varphi(\overrightarrow{r})$ represents a phase term. Harmonic or monochromatic fields are important as they allow to introduce a complex notation whose main consequence is the possibility to eliminate the time dependence from Maxwell equations. The complex representation for the electric field $\overrightarrow{E}(\overrightarrow{r},t)$ can be introduced as follows

$$\begin{aligned}\overrightarrow{E}(\overrightarrow{r},t) &= \overrightarrow{E}_0(\overrightarrow{r})\cos(\omega t + \overrightarrow{\varphi}(\overrightarrow{r})) = \Re\left\{\overrightarrow{E}_0(\overrightarrow{r})\exp(j(\omega t + \overrightarrow{\varphi}(\overrightarrow{r})))\right\} \\ &= \Re\left\{\mathbf{E}(\overrightarrow{r})\exp(j\omega t)\right\} = \Re\left\{\mathbf{E}(\overrightarrow{r},t)\right\} \end{aligned} \tag{2.133}$$

where $\Re\{\cdot\}$ denotes the real part of a complex number. The vector $\mathbf{E}(\overrightarrow{r})$ represents the time independent complex electric field amplitude or simply complex amplitude.

For a monochromatic wave propagating in the direction given by the vector $\overrightarrow{k}$, expressed in a given space coordinate system, the wave equation, Eq. (2.130), is satisfied by any function of the form

$$\Psi(\overrightarrow{r},t) = \Psi_+(\omega t - \overrightarrow{k}\cdot\overrightarrow{r}) + \Psi_-(\omega t + \overrightarrow{k}\cdot\overrightarrow{r}) \tag{2.134}$$

where $\overrightarrow{k} = k\widehat{k}$, $\widehat{k}$ representing the unit vector in the propagation direction and k is the wave number, whose expression is

$$k = \frac{2\pi}{\lambda} = \frac{\omega}{c}. \tag{2.135}$$

The solutions given by Eq. (2.134) are called transversal plane electromagnetic waves or simply TEM waves. Following the IEEE convention [97], the term $(\omega t - \overrightarrow{k}\cdot\overrightarrow{r})$ indicates a wave propagating in the positive sense of the direction given by $\overrightarrow{k}$, whereas the term $(\omega t + \overrightarrow{k}\cdot\overrightarrow{r})$ propagates in the negative sense. For the case of a wave propagating in the positive sense of the vector $\overrightarrow{k}$, the complex electric field amplitude has the form

$$\mathbf{E}(\overrightarrow{r}) = \overrightarrow{E}_0(\overrightarrow{r})\exp(-j\overrightarrow{k}\cdot\overrightarrow{r}). \tag{2.136}$$

For such a this wave, the electric and magnetic fields reside inside the perpendicular plane to $\overrightarrow{k}$. At the same time, the electric and magnetic fields are mutually orthogonal within this plane, which is also known as equiphase plane as all the points on it have the same phase.

Wave Polarization

TEM waves have a transverse vectorial character, which is also known as polarization. Polarimetry characterizes the space-time variation of the electric $\overrightarrow{E}(\overrightarrow{r},t)$ and magnetic $\overrightarrow{B}(\overrightarrow{r},t)$ field vectors. As it is a physical observable, polarimetry is independent of the space coordinate system used to describe it.

Often, the cartesian coordinate system $[\widehat{\mathbf{x}},\widehat{\mathbf{y}},\widehat{\mathbf{z}}]$ is employed to simplify the wave description. In this case, the propagation vector $\overrightarrow{k}$ is chosen collinear to $\widehat{\mathbf{z}}$, therefore, the electric and magnetic fields are confined in the plane defined by the orthogonal vectors $\widehat{\mathbf{x}}$ and $\widehat{\mathbf{y}}$. This is called the wave-oriented coordinate system or *Forward Scattering Alignment* (FSA) convention. For a monochromatic TEM wave, the electric field cartesian components are

$$\overrightarrow{E}(\overrightarrow{z},t) = E_x(\overrightarrow{z},t)\widehat{\mathbf{x}} + E_y(\overrightarrow{z},t)\widehat{\mathbf{y}} = E_{0x}\cos(\omega t - kz - \delta_x)\widehat{\mathbf{x}} + E_{0y}\cos(\omega t - kz - \delta_y)\widehat{\mathbf{y}} \tag{2.137}$$

where δ_x and δ_y represent two constant phase terms. Eq. (2.137) can be also expressed in a vector form

$$\overrightarrow{E}(\overrightarrow{z},t) = \begin{bmatrix} E_x \\ E_y \end{bmatrix} = \begin{bmatrix} E_{0x}\cos(\omega t - kz + \delta_x) \\ E_{0y}\cos(\omega t - kz + \delta_y) \end{bmatrix}. \tag{2.138}$$

The two field components E_x and E_y verify the equation

$$\left(\frac{E_x}{E_{0x}}\right)^2 + \left(\frac{E_y}{E_{0y}}\right)^2 - 2\frac{E_xE_y}{E_{0x}E_{0y}} = \sin^2(\delta) \tag{2.139}$$

where $\delta = \delta_x - \delta_y$. The previous equation gives the locus described by the electric field vector $\overrightarrow{E}(\overrightarrow{z}, t)$ tip along time for any value of z. The electric field tip, describes in the most general case an ellipse, called polarization ellipse, whose shape does not depends neither on time nor space. Fig. 2.12 presents the polarization ellipse for a particular polarization state.

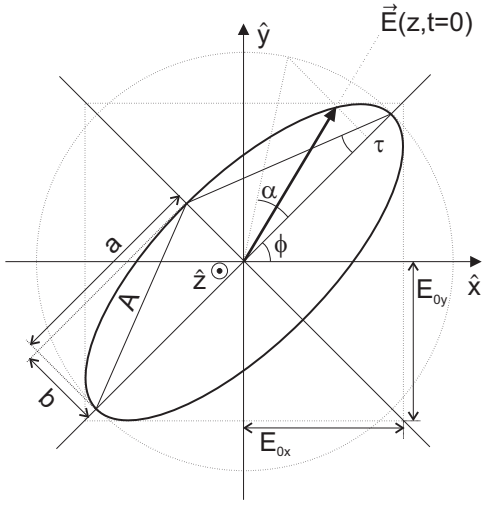

Figure 2.12: Polarization ellipse.

Any elliptic polarization state is defined by the following set of parameters:

- Orientation in space of the polarization ellipse plane. This orientation is given by the polarization ellipse plane normal vector. For the sake of simplicity it is assumed to be $\widehat{\mathbf{z}}$.
- Orientation angle ϕ. This is the angle between the ellipse major axis and the direction defined by the positive $\widehat{\mathbf{x}}$. Its value is in the range $[-\pi/2, \pi/2]$.
- Ellipticity angle τ. This angle represents the ellipse aperture. Its value lies in the range $[-\pi/4, \pi/4]$.

- The polarization sense or handedness. Determines the sense in which the polarization ellipse is described. This parameter is given by the sign of the ellipticity angle τ. Following the IEEE convention [97], the polarization ellipse is right-handed if the electric vector tip rotates clockwise for a wave observed in the direction of propagation, given by $\overrightarrow{k}$. On the contrary, it is said to be left-handed. Therefore, for $\tau < 0$ the polarization sense is right-handed whereas for $\tau > 0$ it is left-handed.
- The polarization ellipse amplitude A. For a major and minor ellipse axes amplitudes a and b respectively, $A = \sqrt{a^2 + b^2}$.
- The absolute phase α representing the initial phase with respect to the phase origin for $t = 0$. It belongs to the range $[-\pi, \pi)$.

Table 2.1 presents the values of the different polarization ellipse parameters for a set of polarization states.

Generally speaking, the polarization state is completely characterized by three independent parameters: the orientation angle, the ellipticity angle (whose sign gives the polarization sense) and the ellipse amplitude.

	Linear horizontal	Linear vertical	Right hand circular	Left hand circular
ϕ	0	$\pi/2$	$[-\pi/2, \pi/2]$	$[-\pi/2, \pi/2]$
τ	0	0	$-\pi/4$	$\pi/4$

Table 2.1: Polarization states.

Wave Polarization Description

As shown before, the polarization state has been described by three independent parameters based on angle measurements. The polarization state can be also described by two different sets of parameters.

As it has been presented, the wave vector components given by Eq. (2.138), can be also expressed by a vector complex formulation

$$\mathbf{E}(\overrightarrow{r},t) = \begin{bmatrix} E_{0x}\exp(j\delta_x) \\ E_{0y}\exp(j\delta_y) \end{bmatrix} \exp(j(\omega t - kz)). \tag{2.140}$$

The real electric field can be recovered by

$$\overrightarrow{E}(\overrightarrow{z},t) = \Re\left\{\mathbf{E}(\overrightarrow{z},t)\right\}. \tag{2.141}$$

A simple wave description can be obtained obviating the propagation term within Eq. (2.140) by evaluating it at $z = 0$ and eliminating the time dependence. In the plane $z = 0$, the electric field $\overrightarrow{E}(z=0)$ can be represented by

$$\mathbf{E}(0) = \mathbf{E}(z=0) = \begin{bmatrix} E_x \\ E_y \end{bmatrix} = \begin{bmatrix} E_{0x}\exp(j\delta_x) \\ E_{0y}\exp(j\delta_y) \end{bmatrix}. \tag{2.142}$$

The vector $\mathbf{E}(0)$ is called the Jones vector of a wave [98, 30, 31, 32]. This vector is a concise complex description of a plane, uniform, monochromatic TEM wave with a given polarization state. The Jones vector only contains information concerning the polarization state as the propagation information has been eliminated. It is worth to mention here, that the Jones vector is a $\mathbb{C}^2$ vector, that is, a two-dimensional complex vector and not a two-dimensional vector in the real space.

The Jones vector describes completely the polarization ellipse shape, as well as the rotation sense of the electric field vector. On the contrary, handedness information can not be included within the Jones vector as it does not contain propagation information. This problem has been solved by introducing the concept of directional Jones vector [99,100,101]. In this case, the propagation direction information is introduced by the symbols '+' and '−', in such a way that $\mathbf{E}_+$ indicates the Jones vector for a wave propagating in the positive sense of $\overrightarrow{k}$, whereas $\mathbf{E}_-$ corresponds to the Jones vector of a wave propagating in the negative sense of $\overrightarrow{k}$. The locus of the polarization ellipse, including the sense of rotation, is independent from the propagation direction. For a Jones vector of a wave propagating in the positive sense of $\overrightarrow{k}$, $\mathbf{E}_+$, the vector $\mathbf{E}_-$ with the same Jones vector but for opposite direction of propagation, has the same locus of the polarization ellipse with the same orientation angle and the same sense of rotation but with opposite ellipticity $\tau_- = -\tau_+$. A Jones vector for a wave propagating in the direction $-\overrightarrow{k}$ with the same polarization is obtained from $\mathbf{E}_+$ by taking the complex conjugate

$$\text{Polarization}\left\{\mathbf{E}_-\right\} = \text{Polarization}\left\{\mathbf{E}_+\right\} \text{ if and only if } \mathbf{E}_- = \mathbf{E}_+^* \tag{2.143}$$

This is true for any linear orthonormal polarization basis. Complex conjugation changes the sign of the phase difference δ and, hence, the sense of rotation but leaves invariant the ellipticity due to the opposite direction of propagation.

Sir G. Stokes, introduced a polarization state description based on four real measurable quantities in the field of optics polarization [102]. These four measurable quantities g_0, g_1, g_2 and g_3, are called the stokes parameters, which are function of the Jones vector components. These four parameters can be arranged in a vector form, leading to the Stokes vector [103, 98]

$$\mathbf{g} = \begin{bmatrix} g_0 \\ g_1 \\ g_2 \\ g_3 \end{bmatrix} = \begin{bmatrix} |E_x|^2 + |E_y|^2 \\ |E_x|^2 - |E_y|^2 \\ 2\Re\left\{E_x^* E_y\right\} \\ 2\Im\left\{E_x^* E_y\right\} \end{bmatrix}. \tag{2.144}$$

As in the case of the Jones vector, the Stokes vector is a polarization state vector and not a polarization vector, as it does not contain wave propagation. Contrary to Jones vector, Stokes vector is a real representation of the polarization state, $\mathbf{g} \in \mathbb{R}^4$. Despite the Stokes vector belongs to $\mathbb{R}^4$, only three components are independent for totally polarized waves

$$g_0^2 = g_1^2 + g_2^2 + g_3^2. \tag{2.145}$$

The stokes parameters g_1, g_2 and g_3 can be interpreted as the cartesian coordinates of a point on a sphere of radius g_0. Therefore, it is possible to map any polarization state to a point of a three dimensional sphere known as the Poincaré sphere [104].

Totally and Partially Polarized Waves

Previously, interest was focused on describing monochromatic waves, whose polarization state does not change in time. These waves are also defined as totally polarized waves. On the other hand, it may happen that the parameters defining the polarization state have a time dependence, i.e.,

$$\mathbf{E} = \begin{bmatrix} E_x \\ E_y \end{bmatrix} = \begin{bmatrix} E_{0x}(t)\exp(j\delta_x(t)) \\ E_{0y}(t)\exp(j\delta_y(t)) \end{bmatrix}. \tag{2.146}$$

In general, the parameters $E_{0x}(t)$, $E_{0y}(t)$, $\delta_x(t)$ and $\delta_y(t)$ will have a random time variation, hence, the polarization ellipse is no longer stable in time. On the contrary, the polarization ellipse has a random variation in shape. Those waves in which the electric field tip describes a trajectory around an average ellipse are called partially polarized waves, whereas those waves in which it describes a complete random trajectory are defined as unpolarized waves [105, 98]. In the latter case, it is not possible to identify an average polarization ellipse.

As the polarization state varies randomly along time, it does no have information for a particular time. On the contrary it is necessary to derive the average polarization state of the wave. Thus, the polarization state, as information source, takes only sense from a statistical point of view. The first consequence of this fact is that only those wave polarization descriptors allowing the introduction of statistics are suitable to describe the wave polarization [105, 98].

The polarization state for totally polarized waves is completely characterized by the Jones vector. This vector is no longer valid to describe partially polarized waves as it varies along time [105, 98]. On the contrary, it is possible to describe the average polarization state of a partially polarized wave by using the wave coherency matrix $[J]$, defined as [98]

$$[J] = E\left\{\mathbf{E}\mathbf{E}^{*T}\right\} = \begin{bmatrix} E\left\{E_x E_x^*\right\} & E\left\{E_x E_y^*\right\} \\ E\left\{E_y E_x^*\right\} & E\left\{E_y E_y^*\right\} \end{bmatrix} \tag{2.147}$$

where $E\{\cdot\}$ represent the statistical expectation. As defined, the wave coherency matrix is a 2 by 2 complex Hermitian matrix containing all the Jones vector second moments.

Partially polarized waves can also be described by the Stokes vector. In this case, as all the stokes vector elements are intensities, it is possible to obtain the average value of these terms

$$\mathbf{g} = \begin{bmatrix} g_0 \\ g_1 \\ g_2 \\ g_3 \end{bmatrix} = \begin{bmatrix} E\left\{|E_x|^2\right\} + E\left\{|E_y|^2\right\} \\ E\left\{|E_x|^2\right\} - E\left\{|E_y|^2\right\} \\ 2E\left\{\Re\left\{E_x^* E_y\right\}\right\} \\ 2E\left\{\Im\left\{E_x^* E_y\right\}\right\} \end{bmatrix}. \tag{2.148}$$

In the case of partially polarized waves, the four stokes parameters are no longer dependent

$$g_0^2 \geq g_1^2 + g_2^2 + g_3^2. \tag{2.149}$$

A partially polarized wave can range from a totally polarized to a totally unpolarized state. The degree of polarization D_p measures the ratio between the totally polarized energy and the total energy of the wave [98]. This parameter can be expressed as a function of the wave covariance matrix elements or as a function of the Stokes vector parameters

$$D_p = \sqrt{1 - \frac{4|[J]|}{tr([J])^2}} = \frac{\sqrt{g_1^2 + g_2^2 + g_3^2}}{g_0} \tag{2.150}$$

where $tr(\cdot)$ denotes the matrix trace. The degree of polarization ranges from 0 to 1. For $D_p = 1$, it means that the wave is completely polarized, whereas for $D_p = 0$ the wave is unpolarized. For any value between 0 and 1, the instantaneous polarization state has an average state.

In the case of an scattered wave by the Earth's surface and recorded by a SAR system, it is important to clarify the concept of wave polarization in this scenario. As presented before, the Earth's surface has been modelled as a set of randomly located point scatterers. For each resolution cell, the recorded wave is the coherent addition of the scattered waves by each of the point scatterers. As the arrangement of point scatterers varies from resolution cell to resolution cell, the received wave polarization state is also random and different from cell to cell. Due to this fact, the received waves can be considered partially polarized in space. Thus, if the goal is to characterize such a scatterer, it has to be done statistically, as this type of analysis will allow to derive the mean scatterer behavior.

2.3.2 Wave Scattering

A single-channel SAR system has been described within Section 2.1. This system is based on sending an EM wave to posteriorly record the scattered version by the Earth's surface. By this process, it is possible to gather information about the surface scattering behavior. This information is the radar cross section, Eq. (2.10), for deterministic or point scatterers, or the scattering coefficient, Eq. (2.65), for random or distributed scatterers.

The complexity increases in the case of PolSAR systems, as more information channels are available. For the case of point scatterers, the polarimetric problem does not present too much difficulties. The problem comes when polarimetry is employed to gather information about distributed scatterers. In this case, the randomness involved within the scattering process makes polarimetric information to be only useful from an statistical point of view. Besides, this randomness will produce PolSAR data to be contaminated by speckle noise. In this case, the speckle noise problem becomes more difficult, as the polarimetric information channels have a correlation degree, which at the same time is an important source of information about the scatterer.

The concept of polarimetric wave scattering can be analyzed from two different perspectives. In both cases, the starting point is the same, an illuminating wave with certain polarization properties. In most of the cases, this wave is totally polarized. On the one hand, it consists in finding the expressions of the scattered fields for a given scatterer. On the other hand, for a given scattered wave, the problem consists in deriving information about the polarimetric properties of the scatterer. The next sections deal with the second of the problems.

2.3.3 The Scattering Matrix

Previous to formally define the scattering matrix, it is important to describe the global scenario in which a PolSAR system images a particular scatterer. First of all, a global cartesian coordinate system $[\hat{\mathbf{x}}, \hat{\mathbf{y}}, \hat{\mathbf{z}}]$ with its origin located within the scattered is defined. All the transverse components of the different fields will be referred to this coordinate system. Without loss of generality, it is possible to assume that the SAR system consists of two antennas, i.e., a transmitting and a receiving antennas, located at any point in the space. When the transmitting and receiving antennas are located in different positions, the

scattering process is referred as forward scattering or bistatic configuration, whereas if both antennas are located at the same point is known as backscattering or monostatic configuration. The transverse electric field vector can be described with two orthogonal polarization states. It will be assumed that these two orthogonal polarization states are the linear horizontal polarization, denoted by $\widehat{\mathbf{h}}$, and the linear vertical polarization, denoted by $\widehat{\mathbf{v}}$, which define the linear polarization basis $\{\widehat{\mathbf{h}}, \widehat{\mathbf{v}}\}$. Therefore, the illuminating field consists of the components E_h^i and E_v^i. The transverse components of the illuminating field are referred to the local coordinate system centered within the transmitting antenna $[\widehat{\mathbf{h}}_i, \widehat{\mathbf{v}}_i, \widehat{k}_i]$. At this point, there exist two different conventions about the definition of the scattered field coordinate system $[\widehat{\mathbf{h}}_s, \widehat{\mathbf{v}}_s, \widehat{k}_s]$. The first convention called *Forward Scattering Alignment* or FSA is defined relative to the propagating wave, therefore it is also known as *wave oriented* coordinate system. The second convention, *Backward Scattering Alignment* or BSA, is defined with respect to the radar antennas in accordance with the IEEE standard [97], which defines the polarization state of an antenna to be the polarization of the wave radiated by the antenna, even when it is used as a receiving antenna. Fig. 2.13 depicts both situations. As a consequence, the equivalences between the coordinate systems of the illuminating and transmitting fields are, for the backscattering direction

$$\begin{array}{cccc} \text{FSA Convention} & & \text{BSA Convention} & \\ \widehat{\mathbf{h}}_s = -\widehat{\mathbf{h}}_i & & \widehat{\mathbf{h}}_s = \widehat{\mathbf{h}}_i & \\ \widehat{\mathbf{v}}_s = \widehat{\mathbf{v}}_i & & \widehat{\mathbf{v}}_s = \widehat{\mathbf{v}}_i & \\ \widehat{k}_s = -\widehat{k}_i & & \widehat{k}_s = \widehat{k}_i & \end{array} \tag{2.151}$$

Under the BSA convention, the illuminating and scattered electric fields components are expressed under the same coordinate system. In order to related both electric fields under the FSA convention, $\widehat{\mathbf{h}}_s = -\widehat{\mathbf{h}}_i$ has to be taken into account. For the BSA convention, assuming the following illuminating and scattered fields

$$\mathbf{E}^i = E_h^i \widehat{\mathbf{h}}_i + E_v^i \widehat{\mathbf{v}}_i \tag{2.152}$$

$$\mathbf{E}^s = E_h^s \widehat{\mathbf{h}}_s + E_v^s \widehat{\mathbf{v}}_s \tag{2.153}$$

it is possible to relate the different field components, under the far field assumption, by a 2 by 2 dimensionless complex matrix of the scatterer, $[S]$, as [105, 67, 27, 26]

$$\begin{bmatrix} E_h^s \\ E_v^s \end{bmatrix} = \frac{\exp(-jkr)}{r} \begin{bmatrix} S_{hh} & S_{hv} \\ S_{vh} & S_{vv} \end{bmatrix} \begin{bmatrix} E_h^i \\ E_v^i \end{bmatrix} \tag{2.154}$$

or equivalently

$$\mathbf{E}^s = \frac{\exp(-jkr)}{r} [S] \mathbf{E}^i \tag{2.155}$$

where r indicates the distance between the scatterer and the receiving antenna, and k is the wavenumber of the illuminating wave. The scattering matrix $[S]$ relates the Jones vector of the illuminating field, a

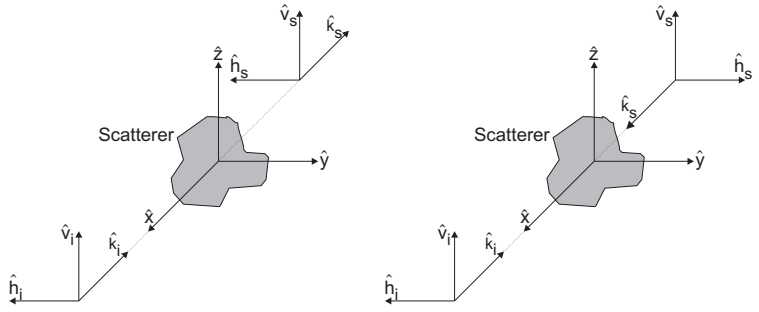

Figure 2.13: Reference system. (a) FSA convention. (b) BSA convention.

wave propagating in the positive sense of $\overrightarrow{k}_i$, with the scattered field Jones vector, a wave propagating in the negative sense of $\overrightarrow{k}_i$. By using the concept of directional Jones vectors, presented within Section 2.3.1 and eliminating the propagation constant, Eq. (2.155) can be written as follows

$$\mathbf{E}^s_+ = [S]\,\mathbf{E}^i_- \tag{2.156}$$
$$\mathbf{E}^s_+ = [S]\,\mathbf{E}^{i\,*}_+ \tag{2.157}$$
$$\mathbf{E}^{s\,*}_- = [S]\,\mathbf{E}^i_-. \tag{2.158}$$

Eq. (2.155), known as field equation, represents the first cornerstone of the polarimetric radar theory. The scattering matrix can be also defined under the FSA convention. Considering $\widehat{\mathbf{h}}_s = -\widehat{\mathbf{h}}_i$

$$[S]_{FSA} = \begin{bmatrix} 1 & 0 \\ 0 & -1 \end{bmatrix} [S]_{BSA}. \tag{2.159}$$

The propagation factor $\exp(-jkr)/r$ is eliminated in the following as it does not affect the polarization information. From now, it will be assumed that $[S]$ is expressed under the BSA convention. Generally, the $[S]$ matrix is referred as the coherent scattering matrix for a bistatic system under the BSA convention. For the monostatic case under the same convention $[S]$ is known as Sinclair matrix, whereas it is referred to the FSA convention $[S]$ is known as Jones matrix.

The scattering matrix elements S_{pq} are called complex scattering amplitudes. These components are understood as the coefficients relating the illuminating field component with $\widehat{\mathbf{q}}$ polarization with the scattered field in $\widehat{\mathbf{p}}$ polarization. These components contain basically the same information as the radar cross section, Eq. (2.10), but introducing polarization dependence and phase information. Indeed, these coefficients are function of frequency, imaging geometry, polarization as well as the physical scattering properties [55, 91].

Up to now, the scattering matrix has been derived for the most general configuration in which the transmitting and receiving antennas are located at different positions. For a monostatic configuration, in which both antennas are located at the same position, some simplifications can be introduced. Through the reciprocity theorem [106, 77], it is possible to derive the following equivalences

$$S_{vh} = S_{hv} \tag{2.160}$$

for the BSA convention, and

$$S_{vh} = -S_{hv} \tag{2.161}$$

for the FSA convention. In general, the bistatic scattering matrix may contain up to seven real independent parameters (four amplitudes and three relative phases). Because of the relations given by Eq. (2.160) or Eq. (2.161), the backscattering scattering matrix contains only up to five real independent quantities (three amplitudes and two relative phases).

The Scattering Vector

As shown by Eq. (2.154), the scattering matrix describes the scattering polarimetric properties by a 2 by 2 complex matrix. This information can be arranged in a vector form, which is known as scattering vector. By a vectorization operator $V([S])$ [107, 108]

$$\mathbf{k}_4 = V([S]) = \frac{1}{2}\mathrm{tr}\,([S]H) = [k_0, k_1, k_2, k_3]^T \tag{2.162}$$

where ^{T} indicates transpose and $tr(\cdot)$ indicates the matrix trace. It is important to note that $\mathbf{k}_4 \in \mathbb{C}^4$. In this case, H is a 2 by 2 complex matrix basis which is constructed as an orthogonal set under the Hermitian inner product. The introduction of the target vector concept will allow to extract polarimetric information from $[S]$ for distributed scatterers [36].

The first orthogonal matrices set H employed to obtain a target vector is the lexicographic basis. In this case, the basis is obtained as the straightforward lexicographic ordering of the elements of $[S]$

$$H_L = \left\{ \begin{bmatrix} 2 & 0 \\ 0 & 0 \end{bmatrix}, \begin{bmatrix} 0 & 2 \\ 0 & 0 \end{bmatrix}, \begin{bmatrix} 0 & 0 \\ 2 & 0 \end{bmatrix}, \begin{bmatrix} 0 & 0 \\ 0 & 2 \end{bmatrix} \right\}. \tag{2.163}$$

Using H_L as a decomposition basis, the scattering vector obtained is

$$\mathbf{k}_{4L} = [S_{hh}, S_{hv}, S_{vh}, S_{vv}]^T. \tag{2.164}$$

This vector $\mathbf{k}_{4L}$ is the conventional scattering vector. Its main advantage is that its elements correspond directly to the scattering matrix entries. The second decomposition basis is the one known as Pauli basis

$$H_P = \left\{ \sqrt{2}\begin{bmatrix} 1 & 0 \\ 0 & 1 \end{bmatrix}, \sqrt{2}\begin{bmatrix} 1 & 0 \\ 0 & -1 \end{bmatrix}, \sqrt{2}\begin{bmatrix} 0 & 1 \\ 1 & 0 \end{bmatrix}, \sqrt{2}\begin{bmatrix} 0 & -j \\ j & 0 \end{bmatrix} \right\}. \tag{2.165}$$

In this case, the obtained scattering vector has the expression

$$\mathbf{k}_{4P} = \frac{1}{\sqrt{2}} [S_{hh} + S_{vv}, S_{hh} - S_{vv}, S_{hv} + S_{vh}, j\,(S_{hv} - S_{vh})]^T. \tag{2.166}$$

The main advantage of the vector $\mathbf{k}_{4P}$ is that its components can be directly related with elementary scattering mechanisms.

One important parameter of the scattering vectors is the norm of the vector $\|\mathbf{k}\|$, which in this case receives the name of span. The span is the total scattered power, therefore it has to be independent from the matrix basis H. For this reason, a factor of 2 and a factor of $\sqrt{2}$ have been included within Eq. (2.163) and Eq. (2.165), respectively. The span is defined as

$$\text{Span}\,([S]) = \|\mathbf{k}_{4L}\|^2 = \mathbf{k}_{4L}\mathbf{k}_{4L}^{*T} = |S_{hh}|^2 + |S_{hv}|^2 + |S_{vh}|^2 + |S_{vv}|^2. \tag{2.167}$$

The scattering vectors, Eq. (2.164) and Eq. (2.166), can be simplified in the backscattering case by [36]

$$\mathbf{k}_{3L} = \left[S_{hh}, \sqrt{2}S_{hv}, S_{vv}\right]^T \tag{2.168}$$

$$\mathbf{k}_{3P} = \frac{1}{\sqrt{2}} [S_{hh} + S_{vv}, S_{hh} - S_{vv}, 2S_{hv}]^T. \tag{2.169}$$

Both vectors belong to $\mathbb{C}^3$. In the case of the vector $\mathbf{k}_{3L}$ a $\sqrt{2}$ coefficient in introduced in order to keep the span.

Scattering Matrix for Distributed Scatterers

Up to this point, interest has been focused on defining the scattering matrix for point scatterers. This type of scatterers are stable in time and/or space. Therefore, the polarimetric properties of the scattered wave do not change in time or space. As both, the illuminating and the scattered waves are totally polarized, the scattering matrix is able to describe the scatterer polarimetric properties. This situation changes radically for distributed or partial scatterers. For a scene model consisting in randomly located point scatterers, it has been shown in Section 2.3.1 that the scattered Jones vector is not able to describe the scattered wave polarimetric properties, since it has a random variation in time and/or space. Thus, since the scattering matrix $[S]$ relates the Jones vector of the illuminating and the scattered waves, this matrix is no longer valid to describe the polarimetric properties of a distributed scatterer, as its components are also random processes.

A polarimetric SAR system measures the four elements of the scattering matrix for each cell of resolution as four complex SAR images. In Section 2.1.4 it was shown that the complex SAR image can

be modelled by $\mathcal{N}_c(0,\sigma^2/2)$, Eqs. (2.55) and (2.56). Hence, the four complex scattering matrix channels can be also modelled as zero-mean, complex, Gaussian pdfs, $\mathcal{N}_c(0,\sigma^2/2)$. The important point in the case of PolSAR data, which was already shown for InSAR data, is the presence of a correlation between the scattering matrix elements.

Assuming $\mathbf{k} = \mathbf{k}_{3L}$ or $\mathbf{k} = \mathbf{k}_{4L}$, the vector $\mathbf{k}$ is described by a multivariate, zero-mean, complex, Gaussian pdf, with the covariance matrix $[C]$ properly defined in each case [109, 21, 22]

$$p_{\mathbf{k}}(\mathbf{k}) = \frac{1}{\pi^Q |[C]|} \exp\left(-\mathbf{k}^{*T}[C]^{-1}\mathbf{k}\right) \tag{2.170}$$

where $Q = 3$ for a monostatic configuration ($\mathbf{k}_{3L}$), whereas $Q = 4$ for a bistatic SAR configuration ($\mathbf{k}_{4L}$). The multivariate, zero-mean, complex, Gaussian pdf presented in Eq. (2.170), and symbolized by $\mathcal{N}(\mathbf{0},[C])$, is completely determined by the complex, Hermitian, positive semidefinite covariance matrix [72], defined as

$$[C] = E\{\mathbf{k}_{3L}\mathbf{k}_{3L}^{*T}\} \tag{2.171}$$

for the monostatic configuration, and

$$[C] = E\{\mathbf{k}_{4L}\mathbf{k}_{4L}^{*T}\} \tag{2.172}$$

for a bistatic configuration. A general theorem for multivariate, complex, Gaussian pdfs states that the nth order central product moment is zero if n is odd, and it is equal to a sum of products of covariances when n is even [110, 72, 111]. As a result, the covariance matrix $[C]$ characterizes completely the statistics of the scattering matrix $[S]$. The matrix $[C]$, contains indeed, power information about the elements of the scattering matrix and information concerning the correlation structure of these elements.

An important point to be mentioned is that $E\{\mathbf{k}\} = 0$, hence, information can not be extracted from $[S]$ in a direct way. In order to obtain information, allowing to characterize the random behavior of the scattering matrix, it is necessary to do it over higher moments, i.e., the covariance matrix.

2.3.4 The Covariance and Coherency Matrices

Most of natural targets, due to their complex structure, can not be considered as perfect scatterers producing totally polarized waves. As a result, this type of scatterers can not be completely characterized by the scattering matrix $[S]$. The logical step to characterize distributed scatterers is to obtain the information of interest from higher moments. This step has been already taken to describe partially polarized waves, see Section 2.3.1, describing them by the stokes vector or by the wave covariance matrix. Hence, distributed scatterers will be described by means of second moments.

The first way to describe partially polarized waves has been to use the real stokes vector. If the polarization properties of the illuminating wave, as well as the properties of the scattered one are described by means of stokes vectors, these vectors can be related by the Müeller matrix $[M]$ [112]. This matrix receives the name of Kennaugh matrix for a monostatic SAR configuration. As it has been done with the EM waves, the Müeller or Kennaugh matrices are able to describe distributed scatterers within the real space.

The second formulation employed to describe the polarization properties of partially polarized EM waves is the complex wave covariance matrix. It is possible to establish a parallel formulation for the distributed scatterers case, describing them by the scatterer, complex, covariance matrix. Using the scattering vector with respect to the lexicographic matrices basis, Eqs. (2.164) or (2.168), the Hermitian, positive semidefinite, scatterer covariance matrix is defined as

$$[C_4] = E\{\mathbf{k}_{4L}\mathbf{k}_{4L}^{*T}\} = \begin{bmatrix} E\{S_{hh}S_{hh}^*\} & E\{S_{hh}S_{hv}^*\} & E\{S_{hh}S_{vh}^*\} & E\{S_{hh}S_{vv}^*\} \\ E\{S_{hv}S_{hh}^*\} & E\{S_{hv}S_{hv}^*\} & E\{S_{hv}S_{vh}^*\} & E\{S_{hv}S_{vv}^*\} \\ E\{S_{vh}S_{hh}^*\} & E\{S_{vh}S_{hv}^*\} & E\{S_{vh}S_{vh}^*\} & E\{S_{vh}S_{vv}^*\} \\ E\{S_{vv}S_{hh}^*\} & E\{S_{vv}S_{hv}^*\} & E\{S_{vv}S_{hv}^*\} & E\{S_{vv}S_{vv}^*\} \end{bmatrix} \tag{2.173}$$

for a bistatic configuration, whereas for a monostatic configuration is

$$[C_3] = E\{\mathbf{k}_{3L}\mathbf{k}_{3L}^{*T}\} = \begin{bmatrix} E\{S_{hh}S_{hh}^*\} & \sqrt{2}E\{S_{hh}S_{hv}^*\} & E\{S_{hh}S_{vv}^*\} \\ \sqrt{2}E\{S_{hv}S_{hh}^*\} & 2E\{S_{hv}S_{hv}^*\} & \sqrt{2}E\{S_{hv}S_{vv}^*\} \\ E\{S_{vv}S_{hh}^*\} & \sqrt{2}E\{S_{vv}S_{hv}^*\} & E\{S_{vv}S_{vv}^*\} \end{bmatrix}. \tag{2.174}$$

The matrices $[C_4]$ and $[C_3]$, as presented in Section 2.3.3, characterize completely the scattering matrix randomness. The advantage of the covariance matrix is that it contains, in a direct way, the Hermitian products between the elements of the scattering matrix. In a similar way, it is possible to define a coherency matrix $[T]$ by using the scattering vector obtained through the Pauli matrices basis [36]. For a bistatic configuration this matrix is defined as

$$[T_4] = E\{\mathbf{k}_{4P}\mathbf{k}_{4P}^{*T}\} \tag{2.175}$$

whereas for a monostatic configuration is

$$[T_3] = E\{\mathbf{k}_{3P}\mathbf{k}_{3P}^{*T}\}. \tag{2.176}$$

The advantage of the coherency matrix it that its elements can be more easily related with simple physical scattering mechanisms.

Both, the conventional scattering vector and the scattering vector obtained from the Pauli basis are derived from the scattering matrix, hence, they contain the same information. In the same way, the covariance and the coherency matrices contain the same information, as they only differ on the way the information is arranged. The equivalences between the covariance and coherency matrices are [36]

$$[T_4] = \frac{1}{2}\begin{bmatrix} 1 & 0 & 0 & 1 \\ 1 & 0 & 0 & -1 \\ 0 & 1 & 1 & 0 \\ 0 & j & -j & 0 \end{bmatrix}[C_4]\begin{bmatrix} 1 & 1 & 0 & 0 \\ 0 & 0 & 1 & -j \\ 0 & 0 & 1 & j \\ 1 & -1 & 0 & 0 \end{bmatrix} \tag{2.177}$$

$$[T_3] = \frac{1}{2}\begin{bmatrix} 1 & 0 & 1 \\ 1 & 0 & -1 \\ 0 & \sqrt{2} & 0 \end{bmatrix}[C_3]\begin{bmatrix} 1 & 1 & 0 \\ 0 & 0 & \sqrt{2} \\ 1 & -1 & 0 \end{bmatrix}. \tag{2.178}$$

The covariance and the coherency matrices are full rank matrices for the case of distributed scatterers, i.e., matrices of rank 4 for a general formulation and rank 3 for the backscattering case. After the expectation process, the symmetric relation between the scattering matrix and the covariance and coherency matrices is lost [36]. This relation is only maintained in the case of point scatterers.

A general 4 by 4 covariance or coherency matrix contains up to sixteen real independent parameters. Equally, for the backscattering case, these matrices contain up to nine independent real parameters. On the other side, the scattering matrix can only contain seven independent parameters in the most general case, whereas only five for the monostatic case. These differences in the number of independent parameters contained in the matrices makes evident the inability of the scattering matrix to describe scattering processes in the case of distributed or partial scatterers. As is has been presented previously, this inability is due to the impossibility of the scattering matrix to describe the correlation properties of its elements.

2.3.5 Covariance Matrix Statistics

For distributed scatterers, the identification and classification of the scatterer structure can only be done by second moments. Section 2.3.3 showed that the conventional scattering vectors, $\mathbf{k}_{3L}$ or $\mathbf{k}_{4L}$ are distributed as $\mathcal{N}(\mathbf{0}, [C_3])$ and $\mathcal{N}(\mathbf{0}, [C_4])$, respectively. The direct link between the scattering matrix $[S]$ and the covariance matrix $[C]$ makes possible to derive the statistics of this matrix. The work presented

in this text is based on describing distributed scatterers by means of the covariance matrix. Hence, only the statistical model of $[C]$ will be presented. As the matrices $[C]$, $[T]$ and $[M]$ are equivalent descriptors for distributed scatterers, it makes sense to analyze one of them, extending the results to the rest.

The covariance matrix is defined on the basis of the expectation operator $E\{\cdot\}$ for wide-sense stationary processes. Therefore, the covariance matrix has to be estimated, i.e., the ensemble average of each of the covariance matrix elements has to be estimated. Under the assumption that the processes S_{pq}, S_{rs} and $S_{pq}S_{rs}^*$ are:

- Wide-sense stationary, i.e., the space averages of each process converge to a finite limit.
- Ergodic in mean, i.e., the different space averages of each process converge to the same limit: the ensemble average.

the ensemble average can be substituted by the spatial average [113]

$$\langle S_{pq}S_{rs}^*\rangle = \frac{1}{N}\sum_{k=1}^{N} S_{pq_k}S_{rs_k}^* \tag{2.179}$$

where N indicates the number of averaged pixels. The previous conditions refer to the calculation of the covariance matrix for wide-sense stationary processes. The first condition is not fulfilled for real SAR images as they are non-stationary processes. Therefore, the stationarity condition has to be relaxed in such a way that the SAR image has to be considered as a locally stationary process. This means that the statistics have to be considered fixed for the local area where the spatial average is calculated, that is, the N pixels belong to the same statistical class. If the process is not locally stationary, the value given by the spatial average is meaningless. As a result, statistics have to be calculated by using a moving window.

The estimation of the covariance matrix elements by averaging the covariance matrices of N pixels is called a multilook process, which is the maximum likelihood estimator of the covariance matrices, Eq. (2.173) or Eq. (2.174). The multilook average presents two important drawbacks. First, the estimated values are clearly dependent on the number of averaged pixels in such a way that the larger the number of averaged pixels the better the covariance matrix estimation [113]. On the other hand, this spatial average process introduces a reduction on the spatial resolution with the clear loss of image details, so that the larger the number of averaged pixels the larger the loss in spatial resolution.

The estimated covariance matrix $[Z]$, for a monostatic SAR configuration in the linear polarization basis $\{\widehat{\mathbf{h}}, \widehat{\mathbf{v}}\}$, is defined as [114, 21, 7, 22]

$$[Z] = \frac{1}{N}\sum_{k=1}^{N}[C_k] = \langle \mathbf{k}_{3L}\mathbf{k}_{3L}^{*T}\rangle = \begin{bmatrix} \langle S_{hh}S_{hh}^*\rangle & \sqrt{2}\langle S_{hh}S_{hv}^*\rangle & \langle S_{hh}S_{vv}^*\rangle \\ \sqrt{2}\langle S_{hv}S_{hh}^*\rangle & 2\langle S_{hv}S_{hv}^*\rangle & \sqrt{2}\langle S_{hv}S_{vv}^*\rangle \\ \langle S_{vv}S_{hh}^*\rangle & \sqrt{2}\langle S_{vv}S_{hv}^*\rangle & \langle S_{hh}S_{vv}^*\rangle \end{bmatrix} \tag{2.180}$$

where $[C_k] = \mathbf{k}_{3L_k}\mathbf{k}_{3L_k}^{*T}$ is the covariance matrix calculated for the kth pixel of the SAR image. The matrix $[Z]$ is often referred as N-look PolSAR data. Based on the multivariate, zero-mean, complex, Gaussian distribution for the target vector $\mathbf{k}$, the estimated covariance matrix $[Z]$ is statistically described by the complex Wishart distribution $\mathcal{W}([C], N)$ [114]

$$p_{[Z]}([Z]) = \frac{N^{QN}\,|[Z]|^{N-Q}\exp\left(-Ntr\left([C]^{-1}[Z]\right)\right)}{K(N,Q)\,|[C]|^{N}} \tag{2.181}$$

where $K(N,Q)$ is the function

$$K(N,Q) = \pi^{(1/2)Q(Q-1)}\Gamma(N)\cdots\Gamma(N-Q+1) \tag{2.182}$$

Q represents the dimension of the vector $\mathbf{k}$. Therefore for a general case $Q = 4$, whereas for the backscattering case $Q = 3$.

An important particular case of the distribution given by Eq. (2.181) is the distribution for one-look imagery, i.e., $N = 1$. In this case, the covariance matrix is simply obtained as the scattering vector Hermitian product for each image pixel. As no estimation process is applied, due to data randomness, it can be stated that useful information, i.e., the average information is damaged by this randomness. As for one-dimensional SAR imagery, this random component is a true electromagnetic measurement known as speckle, but it can only be analyzed by statistical means due to its complexity.

All the covariance matrix elements are the Hermitian product of two scattering matrix elements

$$S_{pq}S_{rs}^{*} = |S_{pq}S_{rs}^{*}| \exp(j(\theta_{pq} - \theta_{rs})) \tag{2.183}$$

where the indices p, q, r and s belong to the orthogonal linear polarization basis $\{\widehat{\mathbf{h}}, \widehat{\mathbf{v}}\}$. Indeed, they could belong to any orthogonal polarization basis, as shown in the following. Besides, the statistical properties of the products $S_{pq}S_{rs}^{*}$ are independent of the number of channels Q. As a result, all the matrix covariance elements share the same statistical properties, allowing to analyze one elements and extending the results to the rest of the covariance matrix elements [21, 22].

2.3.6 Polarimetric SAR Speckle

From Sections 2.3.3 as well as 2.3.5, it follows that PolSAR data can be interpreted as the contribution of two different components. From one side, there is a useful signal component containing information about the scattering process. This information is basically contained within the data average value. On the other hand, these data are damaged by a random contribution, which in this case is also known as speckle noise. Again, it is important to mention that speckle is a true electromagnetic measurement, but it has to be analyzed as a noise-like signal due to the complexity involved within the imaging process.

The most obvious way to find a noise model for the covariance matrix is to extend the multiplicative speckle noise already presented for one-dimensional SAR images, Section 2.1.6. For such a case, each of the scattering matrix elements is assumed to follow

$$S_{pq} = \sqrt{\sigma_{pq}} n_{pq} \exp(j\theta_{pq}) \tag{2.184}$$

where n is the speckle noise, σ_{pq} is the local RCS (proportional to the backscattering coefficient given in Eq. (2.64)) and θ_{pq} represents the true phase measurement. Then

$$\langle S_{pq}S_{rs}^{*} \rangle = \left\langle \sqrt{\sigma_{pq}\sigma_{rs}} \exp(j(\theta_{pq} - \theta_{rs})) \right\rangle \langle n_{pq}n_{rs}^{*} \rangle \,. \tag{2.185}$$

In order to recover the true information from Eq. (2.185) it is necessary that speckle noise averages out, setting $\langle n_{pq}n_{rs}^{*} \rangle = 1$ for $pq = rs$ and zero otherwise. A complex Gaussian variable with this covariance structure is degenerate in the sense that this matrix is a diagonal matrix. This would produce the speckle noise to be the same in all the SAR images, which is not true [7]. Besides, the jointly Gaussian nature has turned out. The non-validity of this extension lies on assuming the SAR channel's phase to be uniformly distributed, which means that posterior uses of the phase are not possible.

InSAR data phase was assumed to be described by an additive phase noise as presented within Section 2.2.3. The previous section presented that InSAR and PolSAR phase differences are described by the same distribution. As in both cases, the data randomness is described by the same distribution, the additive nature of phase noise for InSAR data, can be also extended for PolSAR data. As stated previously, the difference in both cases would be the type of information contained in the average phase. Besides, the phase noise power will depend on the coherence value.

2.3.7 Change of Polarization Basis

Throughout all the previous development, it has been assumed that PolSAR data was referred to the linear orthogonal polarization basis $\{\widehat{\mathbf{h}}, \widehat{\mathbf{v}}\}$. Several reasons can be adduced in favor of this choice. The

first one is the simplicity, in comparison with other possibilities, of the required hardware to work with this set of polarizations. But, the most important reason is the possibility to derive the scatterer response to any polarization state from the response to a pair of orthogonal polarizations [115]. Techniques based on this fact are generally known as polarization basis change techniques. A clear application of them are those methodologies based on looking for the best polarization state for a given goal, as for instance, to look for the polarization state maximizing the returned power [116, 117, 118].

In Section 2.3.1, the polarization state of a electromagnetic wave was described in the polarization basis $\{\widehat{\mathbf{h}}, \widehat{\mathbf{v}}\}$

$$\mathbf{E}_{(\widehat{\mathbf{h}},\widehat{\mathbf{v}})} = \left\langle \mathbf{E}_{(\widehat{\mathbf{h}},\widehat{\mathbf{v}})}, \widehat{\mathbf{h}} \right\rangle \widehat{\mathbf{h}} + \left\langle \mathbf{E}_{(\widehat{\mathbf{h}},\widehat{\mathbf{v}})}, \widehat{\mathbf{v}} \right\rangle \widehat{\mathbf{v}} \tag{2.186}$$

where $\langle \cdot \rangle$ represents the inner product. In a general way, any polarization state can be expressed as the combination of two elliptical polarization state which are orthogonal

$$\mathbf{E}_{(\widehat{\mathbf{u}}_1,\widehat{\mathbf{u}}_2)} = \left\langle \mathbf{E}_{(\widehat{\mathbf{u}}_1,\widehat{\mathbf{u}}_2)}, \widehat{\mathbf{u}}_1 \right\rangle \widehat{\mathbf{u}}_1 + \left\langle \mathbf{E}_{(\widehat{\mathbf{u}}_1,\widehat{\mathbf{u}}_2)}, \widehat{\mathbf{u}}_2 \right\rangle \widehat{\mathbf{u}}_2. \tag{2.187}$$

As a result, if the cartesian basis $\{\widehat{\mathbf{h}}, \widehat{\mathbf{v}}\}$ is denoted by $B1$ and the general elliptical basis $\{\widehat{\mathbf{u}_1}, \widehat{\mathbf{u}_2}\}$ as $B2$, the Jones vector in the basis $B2$ can be obtained as function of the Jones vector in the basis $B1$

$$\mathbf{E}_{B2} = [U_{B1\rightarrow B2}]\, \mathbf{E}_{B1}. \tag{2.188}$$

$[U_{B1\rightarrow B2}]$ is the complex matrix expressing the change of basis. In order to maintain invariant all the wave polarimetric properties, this matrix has to be unitary, i.e., $[U]^{-1} = [U]^{*T}$. It is straightforward, from the previous results, to derive the expression of the scattering matrix $[S]$ given in a different polarization basis. Taking into consideration Eqs. (2.156) to (2.158)

$$\begin{aligned} &\mathbf{E}^s_{+,B1} = [S_{B1}]\mathbf{E}^i_{-,B1} = [S_{B1}](\mathbf{E}^i_{+,B1})^* \Rightarrow \\ &[U_{B2\rightarrow B1}]\mathbf{E}^s_{+,B2} = [S_{B2}][U_{B2\rightarrow B1}]^*(\mathbf{E}^i_{+,B2})^*. \end{aligned} \tag{2.189}$$

By using the properties of the matrix $[U]$, the expression of the scattering matrix in the new polarimetric basis is

$$[S_{B2}] = [U_{B1\rightarrow B2}][S_{B1}][U_{B1\rightarrow B2}]^T. \tag{2.190}$$

The previous equation is defined as the consimilarity transformation [100, 119]. By using the same consideration, it can be demonstrated that a transformation matrix can be also defined for the scatterer vector formulation of the scattering matrix $\mathbf{k}_{4L,B2} = [U_4]\mathbf{k}_{4L,B1}$. All the previous transformations are valid for the case of point scatterers, but it can be extended to distributed scatterers descriptors. The covariance matrix has been defined as the Hermitian product of the scatterer vector, Eqs. (2.172) and (2.171). As a consequence, introducing the basis change matrix $[U_4]$

$$\begin{aligned} [C_{4,B1}] &= E\{\mathbf{k}_{4L,B1}\mathbf{k}^{*T}_{4L,B1}\} = E\{([U_4]\mathbf{k}_{4L,B2})\,([U_4]\mathbf{k}_{4L,B2})^{*T}\} \\ &= [U_4]E\{\mathbf{k}_{4L,B2}\mathbf{k}^{*T}_{4L,B2}\}[U_4]^{*T} = [U_4][C_{4,B2}][U_4]^{*T} \\ [C_{4,B2}] &= [U_4]^{*T}[C_{4,B1}][U_4]. \end{aligned} \tag{2.191}$$

As before, in order to maintain all the polarimetric properties within all the bases, $[U_4]$ is unitary, i.e., $[U_4]^{-1} = [U_4]^{*T}$. Independently of the employed descriptor, the polarimetric basis change matrices are completely deterministic, not being affected by the ensemble average.

2.4 Polarimetric SAR Interferometry

The two previous sections have shown the potential of SAR technology to gather information about the Earth's surface. In this sense, InSAR data are valuable to derive topographic information, whereas PolSAR data give information concerning the nature of the scattering mechanism. In addition to all the

advantages which these two SAR techniques offer, this section is dedicated to present the basics of the technique called Polarimetric SAR Interferometry (PolInSAR) [42, 43, 120].

Apart for terrain topography, InSAR data can be employed to retrieve geo- and bio-physical parameters of the scatterer under observation. The main drawback deriving these parameters is the underestimation of the inversion problem. Several alternatives, in order to increase the system diversity, and therefore to solve the underestimation have been proposed within the literature. These solutions can be classified in the basis of how they increase the number of independent system variables: by temporal diversity [121, 122], by baseline diversity [87, 74, 46] or by frequency diversity [45, 122]. PolInSAR solves the system underestimation by means of using PolSAR data. In addition, all the previous procedures can be combined in order to increase the number of parameters [123, 124, 125].

PolSAR data have been shown as a powerful tool to identify different scattering centers inside a resolution cell by means of the so-called target decomposition techniques [36]. The role of interferometry is, therefore, to locate these scattering centers in the vertical dimension. As a result, the combination of interferometry and polarimetry allows to retrieve scatterer information linked with the vertical dimension. PolInSAR data has been successfully employed for vegetation height estimation [42] or for buried mine detection [126].

2.4.1 Vector Interferometry

An InSAR system measures the terrain complex reflectivity from two slightly different positions, separated by a certain baseline. With this configuration, a scatterer vector has been defined by Eq. (2.105). The Hermitian product of this complex vector allows to extract the information related with the terrain's topography. On the other hand, a PolSAR system measures the scattering matrix $[S]$ for a given resolution cell. The vectorization of the information contained within the scattering matrix, see section 2.3.3, allows to introduce the concepts of covariance and coherency matrices, whose expressions for a monostatic SAR configuration are respectively given by Eqs. (2.174) and (2.176). The covariance and coherency matrices can be extended by using InSAR data. Since this text is based on representing the scatterers by means of the covariance matrix, only the formulation with it will be given. The reader is directed to [42] for the coherency matrix based formulation. To provide a polarimetric SAR system with interferometric capabilities makes possible to extend the ideas of covariance and coherency matrices to cover all the available information. As a result, a PolInSAR system measures the scattering matrices from the same resolution cell from two positions separated by a given baseline. Denoting the scattering vector from the first acquisition point $\mathbf{k}_{3L}$ as $\mathbf{k}_1$ and the corresponding to the second one as $\mathbf{k}_2$, the 6 by 6 Hermitian extended covariance matrix is defined, in a parallel way as it was performed with scalar interferometry, as

$$[C_6] = E\left\{ \begin{bmatrix} \mathbf{k}_1 \\ \mathbf{k}_2 \end{bmatrix} \begin{bmatrix} \mathbf{k}_1^{*T} \mathbf{k}_2^{*T} \end{bmatrix} \right\} = \begin{bmatrix} [C_{11}] & [\Gamma_{12}] \\ [\Gamma_{12}]^{*T} & [C_{22}] \end{bmatrix}. \tag{2.192}$$

The matrices $[C_{11}]$ and $[C_{22}]$ are the standard 3 by 3 complex covariance matrices containing fully polarimetric information for each acquisition. On the contrary, the matrix $[\Gamma_{12}]$ contains interferometric as well as polarimetric information. The diagonal of this matrix contains the interferograms obtained with each one of the orthogonal polarizations, as well as the interferogram obtained with the cross-polar polarimetric terms. The rest of the Hermitian terms contain polarimetric as well as interferometric information by means of crossed terms.

As it has been presented throughout all this chapter, SAR data for distributed or partial scatterers are characterized by a random behavior called speckle, that, despite being a true electromagnetic measurement, acts as a noise-like signal, making useful information to have sense only from a statistical point of view. As a consequence, this useful information has to be estimated from the real SAR data. PolInSAR data is also affected by the noise-like speckle. Within section 2.1.4, it was demonstrated that each SAR image can be independently described by a zero-mean, complex, Gaussian pdf $\mathcal{N}_c(0, \sigma^2/2)$.

Sections 2.2.3 and 2.3.3 showed that the scatterer vectors, independently of the information content, can be modelled as a zero-mean, multivariate, complex Gaussian pdf $\mathcal{N}(\mathbf{0}, [C])$, completely characterized, from a statistical point of view, by a covariance matrix. This matrix contains all the second moments of the scattering matrix elements. As a consequence, the extended scattering vector, defined as $[\ \mathbf{k}_1 \quad \mathbf{k}_2\ ]^T$ is modelled by a six-dimensional, zero-mean, complex, Gaussian pdf $\mathcal{N}(\mathbf{0}, [C_6])$. This distribution, as for the InSAR and PolSAR data cases, is characterized, for a monostatic radar configuration, by a 6 by 6 covariance matrix. This matrix is precisely the extended matrix shown by Eq. (2.192).

Equally as for PolSAR data, as the covariance matrix contains all the useful information, it is necessary to estimate it, i.e., speckle noise has to be reduced. Therefore, the extended covariance matrix will be also described by the Wishart distribution, Eq. (2.181), but taking into consideration that it now reflexes six-dimensional data. Despite the dimension increase, all the extended covariance matrix elements will share the same statistical properties, already presented within section 2.3.5. The first consequence of this parallelism, is that there is not a speckle noise model for the extended covariance matrix.

2.4.2 Information Extraction

For natural targets, PolInSAR data is completely determined by the complex 6 by 6 extended covariance matrix. The different information products contained in this matrix can be extracted by defining two normalized complex vectors $\mathbf{w}_1$ and $\mathbf{w}_2$ [42], which can be interpreted as two scattering mechanisms characterized by a single scattering matrix [36]. This two vectors are employed as projection vectors, that is, the scattering vectors $\mathbf{k}_1$ and $\mathbf{k}_2$ are respectively projected over $\mathbf{w}_1$ and $\mathbf{w}_2$

$$u_1 = \mathbf{w}_1^{*T}\mathbf{k}_1 \quad u_2 = \mathbf{w}_2^{*T}\mathbf{k}_2 \ . \tag{2.193}$$

The terms u_1 and u_2 are therefore combinations of the scattering vector elements, $\mathbf{k}_1$ and $\mathbf{k}_2$. The role of the vectors $\mathbf{w}_1$ and $\mathbf{w}_2$ is just to extract the information of interest from the PolInSAR data in order to define InSAR data out from the extended covariance matrix. If u_1 and u_2 are written in a vector, as it was done in Eq. (2.105), the expected Hermitian product, allowing to extract interferometric information, is

$$[C] = E\left\{ \begin{bmatrix} S_1 \\ S_2 \end{bmatrix} [S_1^* S_2^*] \right\} = \begin{bmatrix} \mathbf{w}_1^{*T}\,[C_{11}]\,\mathbf{w}_1 & \mathbf{w}_1^{*T}\,[\Gamma_{12}]\,\mathbf{w}_2 \\ \mathbf{w}_2^{*T}\,[\Gamma_{12}]^{*T}\,\mathbf{w}_1 & \mathbf{w}_2^{*T}\,[C_{22}]\,\mathbf{w}_2 \end{bmatrix} . \tag{2.194}$$

This matrix has the same properties as Eq. (2.107). The diagonal elements of the previous matrix contain the intensities of the SAR images S_1 and S_2 obtained as a projection of the PolSAR data over the scattering mechanisms $\mathbf{w}_1$ and $\mathbf{w}_2$. On the contrary, the off-diagonal elements contain the Hermitian products combining the scattering mechanisms $\mathbf{w}_1$ and $\mathbf{w}_2$. As the scattering mechanisms $\mathbf{w}_1$ and $\mathbf{w}_2$ are different, the information contained within the off-diagonal elements is affected by interferometric as well as polarimetric contributions. Therefore, the phase of the correlation coefficient will be affected by the topography but also by polarimetric contributions. Finally, the amplitude of the correlation coefficient, or interferometric coherence, can be split into [123]

$$\rho = \rho_{int}\,\rho_{pol}. \tag{2.195}$$

The term ρ_{int} accounts for all the interferometric coherence terms presented within section 2.2.4, whereas ρ_{pol} accounts for the polarimetric coherence terms. Only when $\mathbf{w}_1 = \mathbf{w}_2$, ρ_{pol} becomes one, and ρ only accounts for interferometric coherence terms.